

Prepared in cooperation with the U.S. Fish and Wildlife Service

Effects of Proposed Sediment Borrow Pits on Nearshore Wave Climate and Longshore Sediment Transport Rate Along Breton Island, Louisiana

By P. Soupy Dalyander, Rangley C. Mickey, Joseph W. Long, and James Flocks

Open-File Report 2015–1055

U.S. Department of the Interior
SALLY JEWELL, Secretary

U.S. Geological Survey
Suzette M. Kimball, Acting Director

U.S. Geological Survey, Reston, Virginia: 2015

For more information on the USGS—the Federal source for science about the Earth, its natural and living resources, natural hazards, and the environment—visit <http://www.usgs.gov> or call 1–888–ASK–USGS

For an overview of USGS information products, including maps, imagery, and publications, visit <http://www.usgs.gov/pubprod>

Any use of trade, firm, or product names is for descriptive purposes only and does not imply endorsement by the U.S. Government.

Although this information product, for the most part, is in the public domain, it also may contain copyrighted materials as noted in the text. Permission to reproduce copyrighted items must be secured from the copyright owner.

Suggested citation:

Dalyander, P.S., Mickey, R.C., Long, J.W., and Flocks, James, 2015, Effects of proposed sediment borrow pits on nearshore wave climate and longshore sediment transport rate along Breton Island, Louisiana: U.S. Geological Survey Open-File Report 2015–1055, 41 p., <http://dx.doi.org/10.3133/ofr20151055>.

Contents

Abstract	1
Introduction.....	1
Background	2
Methods.....	4
Wave Climatology.....	4
Numerical Model.....	6
Borrow Pit Designs	7
Wave Impact Analysis.....	8
Results.....	11
Numerical Model Assessment	11
Sensitivity Analysis	18
Effects of Borrow Pits on Nearshore Wave Climate and Longshore Transport	21
Conclusions.....	24
Acknowledgments	25
References Cited	25
Appendix 1. Scenarios.....	29
Appendix 2. Example Model Input Files	32
Appendix 3. File Naming Conventions	41

Figures

1. Maps showing the location of Breton Island in the Gulf of Mexico, the G1, G2, and G3 numerical model domains, and the three National Data Buoy Center buoys used in model scenario development and assessment; and the spatial extent of the G3 model domain, showing the G4 domain as well as the extent of two proposed borrow pits considered in the wave modeling study	2
2. Wave bins used to establish the wave climatology at National Data Buoy Center buoy 42040	5
3. Two proposed borrow pit designs evaluated for the impact to the wave climate around Breton Island.....	7
4. Portion of G4 showing the 135 cross-shore transects used in calculating the alongshore flux	10
5. Depth at which depth-induced wave breaking dissipation exceeded 0.01 watt per square meter at 95 percent of alongshore locations for each wave scenario	10
6. Comparison of the Simulating WAVes Nearshore grid G1 and WavewatchIII® model output of significant wave height, peak wave period, and mean wave direction versus observations at National Data Buoy Center buoys 42040, 42012, and 42007	12
7. Comparison of Simulating WAVes Nearshore and WavewatchIII® G2 model output of significant wave height, peak wave period, and mean wave direction versus observations at National Data Buoy Center buoys 42012 and 42007 for each scenario	13
8. Time series above shows a portion of the entire probabilistic wave reconstructed time series at buoy 42012 comparing the observations, reconstructed values, and measurement at offshore buoy 42040.....	16
9. Time series above shows a portion of the entire probabilistic wave reconstructed time series at buoy 42007 comparing the observations, constructed values, and measurement at offshore buoy 42040	17

10.	Comparison of wave time series constructed using probabilistic method and observations at National Data Buoy Center buoy 42012 for April 2, 2010, to December 30, 2013, and comparison of the WavewatchIII® dataset and the observations for the same time period.....	17
11.	Comparison of wave time series constructed using probabilistic method and observations at NDBC buoy 42007 for the time period January 19, 2005, to February 15, 2008, and comparison of the WavewatchIII® dataset and the observations for the same time period.....	18
12.	Model sensitivity to wave diffraction in grid G4 with pit 1 present for scenario H6_D7	19
13.	Model sensitivity to wave triads in grid G4 with pit 1 present for scenario H6_D7	20
14.	Weighted average significant wave height for the baseline, no pit bathymetry, bathymetry including borrow pit 1, and bathymetry including borrow pit 2	21
15.	For 135 locations along Breton Island, longshore transport rate for each of the 116 wave scenarios for the no pit case	22
16.	For 135 locations along Breton Island, change in the longshore transport rate with the addition of pit 1 and pit 2 for each of the 116 wave scenarios	22
17.	For 135 locations along Breton Island, gradient of average longshore transport rate calculated by weighting each of the 116 individual scenario results by its frequency of occurrence in the wave climatology..	23
18.	Gradient of average longshore transport rate constructed from the longshore transport calculated using wave conditions at 135 locations along Breton Island for each of the 116 individual scenario results by weighting each scenario by its frequency of occurrence in the wave climatology	24

Tables

1.	Dimensions of the proposed borrow pits designed for the modeling scenarios.....	8
2.	Comparison of the Simulating WAVes Nearshore model output from grids G1 and G2 to WavewatchIII® model output evaluated against observed buoy data from the representative time step of each scenario	13
3.	Reconstruction performance and error statistics using the 116 unique scenarios generated for grid G2.	15

Conversion Factors

SI to Inch/Pound

Multiply	By	To obtain
Length		
centimeter (cm)	0.3937	inch (in.)
meter (m)	3.281	foot (ft)
kilometer (km)	0.6214	mile (mi)
Density		
kilogram per cubic meter (kg/m ³)	0.06242	pound per cubic foot (lb/ft ³)

Vertical coordinate information is referenced to the North American Vertical Datum of 1988 (NAVD 88)

Horizontal coordinate information is referenced to the World Geodetic System 1984 (WGS84)

Elevation, as used in this report, refers to distance above the vertical datum.

Effects of Proposed Sediment Borrow Pits on Nearshore Wave Climate and Longshore Sediment Transport Rate Along Breton Island, Louisiana

P. Soupy Dalyander, Rangley C. Mickey, Joseph W. Long, and James Flocks

Abstract

As part of a plan to preserve bird habitat on Breton Island, the southernmost extent of the Chandeleur Islands and part of the Breton National Wildlife Refuge in Louisiana, the U.S. Fish and Wildlife Service plans to increase island elevation with sand supplied from offshore resources. Proposed sand extraction sites include areas offshore where the seafloor morphology suggests suitable quantities of sediment may be found. Two proposed locations east and south of the island, between 5.5–9 kilometers from the island in 3–6 meters of water, have been identified. Borrow pits are perturbations to shallow-water bathymetry and thus can affect the wave field in a variety of ways, including alterations in sediment transport and new erosional or accretional patterns along the beach. A scenario-based numerical modeling strategy was used to assess the effects of the proposed offshore borrow pits on the nearshore wave field. Effects were assessed over a range of wave conditions and were gaged by changes in significant wave height and wave direction inshore of the borrow sites, as well as by changes in the calculated longshore sediment transport rate. The change in magnitude of the calculated sediment transport rate with the addition of the two borrow pits was an order of magnitude less than the calculated baseline transport rate.

Introduction

North Breton Island, located at the southern end of the Chandeleur Islands, Louisiana, and part of the Breton National Wildlife Refuge (BNWR), provides important habitat for nesting colonies of brown pelicans. Loss of subaerial island extent can affect this species through reduction of nesting area. Due to storm impacts, relative sea level rise, and diminished sediment supply from dredging of the Mississippi River Gulf Outlet (MRGO), island area has been reduced by 93 percent since the 1920s (Martinez and others, 2009). In an effort to preserve Breton Island (fig. 1), the southernmost extent of the BNWR, the U.S. Fish and Wildlife Service (FWS) plans to nourish the island by restoring island elevation using nearby offshore sand resources. FWS requested that the U.S. Geological Survey (USGS) evaluate the potential effects of mining offshore sand on the wave climate and longshore sediment transport at Breton Islands; results of that evaluation are presented in this report. Studies have shown that sediment deposits within BNWR suitable for shoreline nourishment are rare (Twichell and others, 2009) and are confined to buried distributary channels, terminal spits, and tidal deposits (Flocks and others, 2009). Analyzing the seafloor morphology offshore of Breton Island, potential relict spit and tidal deposits have been identified in approximately 3–6 m of water. Dredging borrow pits in these deposits will change the seafloor morphology, which could alter the wave transformation and result in changes in the wave climate locally and around the island. If effects on the wave climate extend to nearshore regions around the island, the breaking wave characteristics (significant height and peak wave direction), which dictate alongshore sediment transport magnitude and direction, could be altered. Changes in sediment

transport processes may alter patterns in erosion or accretion with implications for the planned nourishment of the island. To evaluate these potential effects, two proposed borrow pits within the suitable offshore deposits have been positioned in a numerical model to evaluate the impact on wave dynamics. The goal of the effort is to employ a scenario-based approach to quantify what effects the proposed borrow pit designs would have on the nearshore wave climate at Breton Island by considering the entire range of wave conditions in the region.

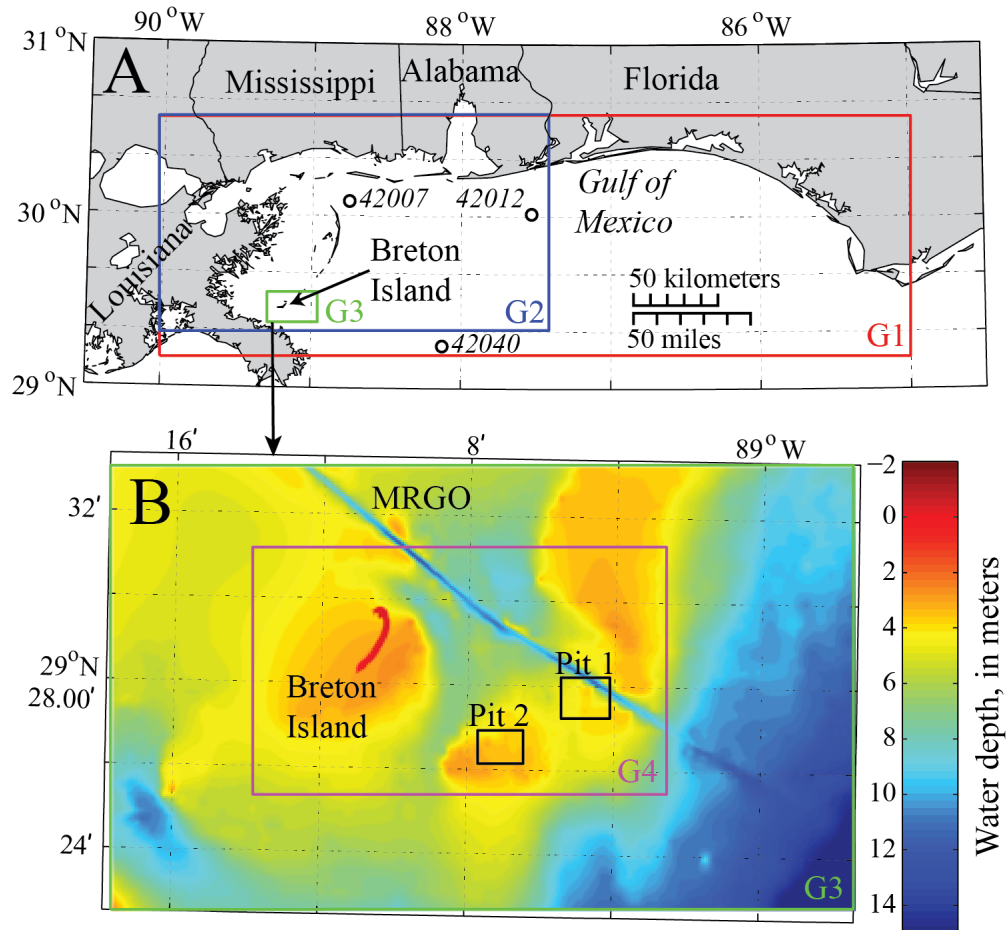


Figure 1. Maps showing (A) the location of Breton Island in the Gulf of Mexico, the G1, G2, and G3 numerical model domains, and the three National Data Buoy Center (NDBC) buoys (42040, 42012, and 42007) used in model scenario development and assessment, and (B) the spatial extent of the G3 model domain, showing the G4 domain as well as the extent of two proposed borrow pits considered in the wave modeling study. The channel running northeast of Breton Island is the Mississippi River Gulf Outlet (MRGO).

Background

The potential effects of borrow sites at any given location will depend on the local bathymetry, geology, wave climate, and borrow pit design. As waves enter intermediate to shallow water depths, that is, depths less than approximately half the wavelength of the surface gravity waves, they begin to interact with the seafloor and as a result undergo several transformation processes including shoaling, refraction, diffraction, reflection, and dissipation (Komar, 1998). Perturbations such as borrow pits can

alter the wave field to varying degrees through each of these processes. In wave refraction, the direction of wave propagation rotates such that wave crests align to be more parallel with depth contours. Depending on the configuration of the borrow pit and its orientation relative to the bathymetry contours, waves will refract around the edges of the pit in various directions resulting in a divergence or convergence of wave energy (Komar, 1998; Bender and Dean, 2003). Diffraction transfers energy along the wave crest from high wave height to low wave height, resulting in complex patterns in the lee of alongshore perturbations to the wave field such as breakwaters or borrow pits (Komar, 1998). Diffraction typically results in relatively minor impact to the wave field compared to refraction (Demir and others, 2004); however, excluding the effects of diffraction may result in overprediction of shoreline changes as a result of wave field modification (Benedet and List, 2008). The reflection of wave energy off the borrow pit perturbation results in a reduction of wave energy transmission onshore of the borrow pit (Demir and others, 2004) and is a larger factor during storm wave conditions than under calmer wave conditions (Michelsen and others, 2008). Refraction, diffraction, and reflection are all processes of wave scattering; in contrast, wave dissipation is the process by which wave energy is lost through breaking or frictional interaction with the seafloor. In the case of borrow pits, the depth increase reduces the wave energy bottom dissipation at that location, increasing the wave energy (and wave heights) leeward of the pit (Komar, 1998).

Borrow pits placed in shallow, nearshore areas may directly alter the sediment budget along coastlines by trapping sediment that would otherwise be transported across that location. These effects are assumed to be minimal if the pits are located beyond the site-specific closure depth, an engineering criterion beyond which sediment mobility is considered limited (Bender and Dean, 2003); however, depth of closure may not adequately capture the disproportionate impact of infrequent storm events (Kennedy and others, 2009; Gonçalves and others, 2014). The aforementioned changes to the wave environment can alter sediment transport patterns and morphology along the coastline of areas in the lee of borrow pits particularly as a result of changes in wave-induced alongshore currents. The complexity of wave transformation processes and the resultant convergences and divergences of wave energy can create a site-specific shoreline response if the wave variations extend to the surf zone where waves break because of limited water depth and wave momentum is transferred into cross-shore and alongshore currents. In some cases, the shoreline in the lee of the pit accretes, resulting in a salient behind the pit with adjacent areas of erosion (Combe and Soileau, 1987; Bender and Dean, 2003). In other cases, erosional “hot spots” develop directly shoreward or offset to one side of the pit (depending on predominant wave direction), with the eroded sand transported alongshore (Wang and Dean, 2001; Bender and Dean, 2003; Benedet and List, 2008) or possibly cross-shore (Kraus and Galgano, 2001). Alternately, if the borrow pit is far enough offshore and in deep enough water, effects to the coastline may be minimal (Maa and Hobbs, 1998; Byrnes and others, 2004; Zarillo and others, 2009).

The impact a borrow pit will have on the wave field and adjacent shoreline depends on the seafloor geology, wave climate, and design characteristics of the pit such as distance offshore, depth of cut, orientation, and cross- and alongshore extent (Benedet and others, 2013). Because the seafloor geology and wave climate are relatively fixed for any given site, sensitivity analysis has typically focused on design characteristics. The farther from shore a borrow pit is located and the deeper the water depth, the smaller the impact will be to the adjacent shoreline; however, the increased cost of sediment extraction farther from shore may prohibit extraction beyond a certain depth (Benedet and others, 2013). Borrow pits designed as narrow alongshore trenches, thus minimizing the cross-shore length of wave effects, may have a limited impact on wave climate compared to pits with a more square profile (Benedet and others, 2013).

A synopsis of the various approaches that have been used to assess the effects of borrow pits on waves and adjacent shorelines can be found in Bender and Dean (2003) and is only briefly reviewed here. These approaches include field and laboratory experiments, as well as the use of analytical 1-D and 2-D models. In addition, parabolic and elliptic numerical models (RCPWAVE, REF/DEF, MIKE 21 EMS Module) and wave-action balance equation models (SWAN, STWAVE) have been used (Bender and Dean, 2003). In the 10 years since the Bender and Dean (2003) study, increases in computer power have resulted in more applications of wave spectra-resolving numerical models, such as SWAN or CMS-WAVE and high-fidelity, and 2-D or 3-D models with sediment transport modules, such as Delft 3-D, to the assessment of the effects of borrow pits on the wave climate, alongshore currents, and nearshore sediment transport (Benedet and others, 2007; Benedet and List, 2008; Hartog and others, 2008; Benedet and others, 2013).

Methods

Wave conditions in the northern Gulf of Mexico around Breton Island were quantified using an approach developed by Long and others (2014). In this methodology, the wave climatology at any given location is characterized into a discrete set of scenarios, which are subsequently numerically modeled to provide the spatial variability over the domain of interest in wave conditions represented by that scenario. The methodology and its application here are described in more detail in the section “Wave Climatology,” and the numerical model used to construct the scenarios is described in “Numerical Model.” This approach was used to investigate the effects of two possible configurations of offshore sand extraction, described in “Borrow Pit Designs,” with the resultant effects on the wave climate quantified in an approach described in “Wave Impact Analysis.”

Wave Climatology

In the application of the wave-scenario approach, waves at National Data Buoy Center (NDBC) buoy 42040 over the time period December 1995 through December 2013, the time range of consistent buoy operation, were used to build a wave climatology for the northern Gulf of Mexico by weighted averaging a set of representative scenarios. Hourly wave observations were divided into a discrete set of bins by significant wave height and mean wave direction. Eight significant wave height bins of width ranging from 0.5 to 1 meter (m) and 16 wave direction bins of width 22.5 degrees (°) were used (fig. 2). For each bin (appendix 1), a single representative time was chosen when the wave height and direction at buoy 42040 most closely matched the wave height and direction averaged over all observational times assigned to that bin. Because forcing conditions were provided by the National Oceanic and Atmospheric Administration (NOAA) operational WAVEWATCH III® model (<http://polar.ncep.noaa.gov/waves/index2.shtml>), an additional constraint was imposed that at the selected representative time step for each bin the error in significant wave height and wave direction for WAVEWATCH III® at buoy 42040 could be no more than 20 percent of the observed value at the buoy. The wave model was then run for each of these conditions to simulate the spatial variability of waves within the study area. Wave period, wind speed, and wind direction were not explicitly matched using this approach; however, Bayesian analysis that identifies the best matched times using significant wave height, peak wave period, peak wave direction, and wind speed showed only minor variation in the time periods chosen. Using the two methods to hindcast complete wave time series showed only minor improvement in predicting significant wave height and peak period and a slight decrease in the prediction of wave direction (Plant and others, 2013; Long and others, 2014). Analysis of the overall accuracy of the model in this study is

presented with the results. The primary benefit of scenario-based modeling for this application is that the use of deterministic modeling to capture wave conditions over multiannual time scales in terms of computational expense would be prohibitive, while modeling over a shorter time scale might not capture truly representative conditions. A complete description of this wave-scenario approach and its application can be found in Long and others (2014); the current study increased the number of bins from 80 to 116 to better resolve the variability of larger wave heights (waves >2 m, fig. 2).

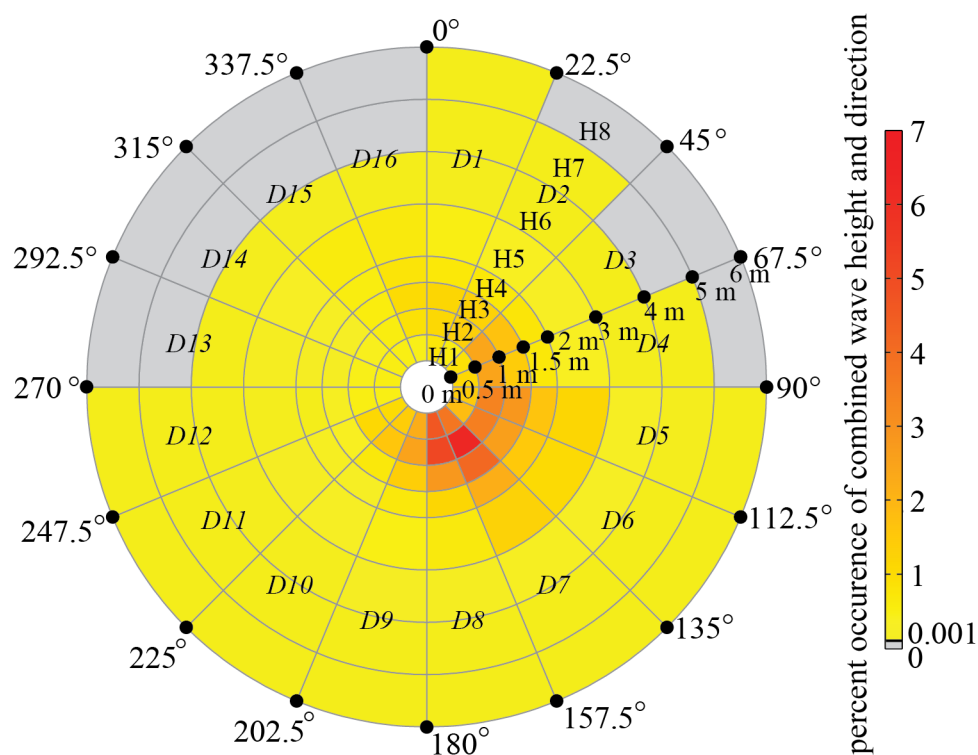


Figure 2. Wave bins used to establish the wave climatology at National Data Buoy Center (NDBC) buoy 42040 (fig. 1). A total of 16 wave direction bins (D1–D16) and 8 wave height bins (H1–H8) were used to discretize the observations. Of the 128 direction and height bins, 12 contained no observations, indicated in gray, leaving 116 model scenarios. For the other wave bins, colors indicate the percentage of observations falling within that bin for the time period December 1995 through December 2013, with values ranging between 0.001–6.3 percent. [m, meters]

Waves at buoy 42040 were most often out of the southeast with wave height less than 1.5 m (fig. 2). The largest storm wave conditions, with wave heights greater than 4 m, were also out of the south and southeast and commonly were associated with tropical storm events. A total of 12 bins out of the 128 wave height and direction combinations, all representing northerly waves of greater than 4 m, did not contain observations; therefore, 116 scenarios were used to capture the wave climatology at this site.

The scenario-based wave modeling approach allowed for the spatial variability in wave conditions (and longshore flux) to be estimated for a given offshore wave height and direction. By using the percentage occurrences computed for each wave condition (fig. 2), a weighted average of the scenario results for a variable of interest was created. This weighted averaging technique, applied to significant wave height and longshore transport rates, was used to quantify changes in wave and sediment transport conditions around Breton Island for the two borrow pits.

Numerical Model

The Simulating WAVes Nearshore (SWAN) numerical wave model (version 41.01; Booij and others, 1999; Ris and others, 1999; The SWAN Team, 2014) was used to characterize wave conditions for each scenario. A system of four one-way nested grids was constructed (fig. 1): G1 covered the northern Gulf of Mexico from Louisiana to western Florida at 1,500 m resolution; G2 covered the western half of the G1 domain from Louisiana to Alabama at 300 m resolution; G3 covered Breton Island and the surrounding offshore at 60 m resolution; and G4 focused on Breton Island itself and the proposed offshore borrow pits at 20 m resolution with an increased cross-shore resolution of 10 m in the near-shore region and over the island. Bathymetry for grids G1, G2, and G3 were provided by the NOAA National Geophysical Data Center (NGDC) Northern Gulf Coast digital elevation model (DEM) (Love and others, 2012). Bathymetric and topographic elevations for grid G4 were derived from the NGDC Northern Gulf Coast DEM, regional bathymetry collected in 2006–07 described by Miner and others (2009), and a 2014 topographic/bathymetric light detection and ranging (lidar) survey contracted by the U.S. Geological Survey. These elevations were merged and interpolated to the G4 grid using the scale-controlled interpolation method of Plant and others (2002). Wave boundary conditions for the G1 model at the open boundaries are prescribed from archived operational output of the NOAA WavewatchIII® 4-minute (~7.5 kilometer) resolution U.S. east coast multigrid (Tolman, 2008) using wave height, peak period, and peak direction with an assumed Joint North Sea Wave Project (JONSWAP) spectrum (Hasselmann and others, 1973). Wind forcing for all of the model grids was also provided by archived model output from the same WavewatchIII® grid.

For each scenario, SWAN was run in stationary mode with a frequency range of 0.04–1.0 hertz (Hz), with frequency spacing of 0.1 times the frequency. Directional resolution was 6° over the full 360°. Minimum depth values were set at 0.2 m for G1 and G2, and 0.05 m for G3 and G4. Third generation Komen physics (Komen and others, 1984), including wind generation and whitecapping, were used for all simulations with parameterizations following Rogers and others (2003) to reduce inaccurate attenuation of swell energy by whitecapping. A default parameterization of JONSWAP (Hasselmann and others, 1973) bottom friction with $0.067 \text{ m}^2\text{s}^{-3}$ roughness was used, consistent with other applications of the SWAN or Delft3-D application to assess the effects of borrow pits on waves and alongshore transport (Benedet and others, 2007; Benedet and List, 2008; Hartog and others, 2008). The backward space backward time (BSBT) finite difference scheme was employed. Quadruplet computations were included using the default discrete interaction approximation (DIA) method for nonlinear 4-wave interactions (The SWAN Team, 2014). Depth-induced breaking following the Battjes and Janssen (1978) parameterization was included with default values for alpha (1) and gamma (0.73). Sensitivity testing was conducted to determine if triad wave interaction and wave diffraction needed to be activated in the model. Triad interactions are non-linear wave transformations in shallow water that result in transfer of energy across different frequencies, changing the shape of the wave spectra (Madsen and Sørensen, 1993; Booij and others, 1999). A more complete description of this analysis is found in the section “Results.” Diffraction did not significantly influence the wave model output, although triad wave interactions were found to be important and were activated in grids G3 and G4, using the default SWAN values of 0.1 for the proportionality constant, a maximum frequency cutoff of 5, a critical Ursell number of 0.2, and a lower threshold Ursell number of 0.01. For grids G1–G3, the SWAN NESTOUT command was used to generate the boundary condition files for the next higher resolution grid (grids G2–G4). Examples of input files for each of the four grids are provided in appendix 2.

Borrow Pit Designs

Two possible borrow pit designs, targeting potential sediment resources suitable for shore-line nourishment, were considered for their potential effects to the wave climate around Breton Island (fig. 3). Historical nautical charts of the area reveal geomorphic features that may contain sandy material: ebb-tide shoals associated with Breton Island Pass prior to the excavation of the MRGO and possible terminal spit deposits that may be related to former southward progradation of the northern Chandeleur barrier platform during the transgressive evolution of the islands seaward of the Breton Island platform. In addition, geophysical investigations indicate that distributary channels of the former St. Bernard delta are preserved in the subsurface in this area and may contain suitable sand deposits (Twichell and others, 2009). Because these deposits are located 5–10 km offshore of the Breton Island platform, with intervening deeper water, they are unlikely to contribute to the natural sediment budget of the island. Use of these deposits would contribute beneficially to the island’s sediment budget if the sediments were placed on the island or within the littoral system. Finally, the proposed borrow pits were positioned between the island and the prevailing wave direction to provide a scenario where affected wave action would have the most impact on the island platform.

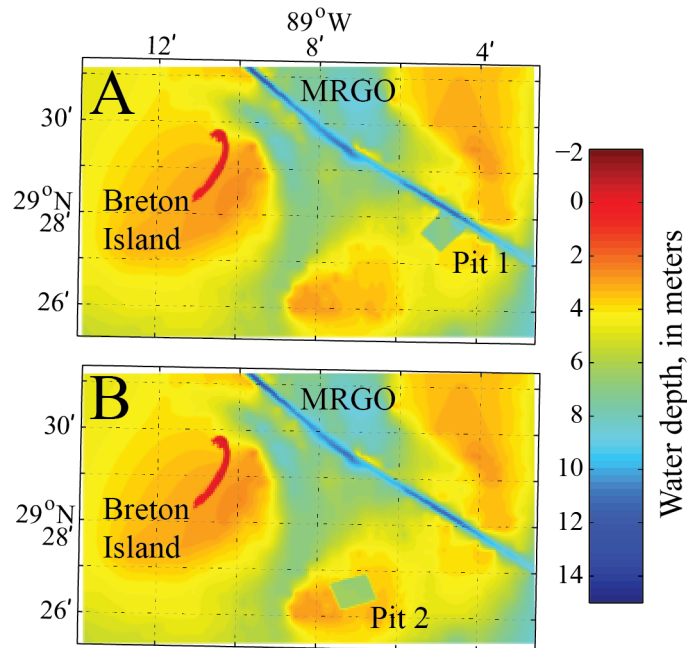


Figure 3. Two proposed borrow pit designs evaluated for the impact to the wave climate around Breton Island. [MRGO, Mississippi River Gulf Outlet]

The thickness and extent of the offshore deposits are not known. Because the borrow pit design is intended for evaluating wave scenarios, the borrow design was adapted from the closest fully designed, evaluated, and implemented borrow pit in the area. In 2011 a borrow pit was excavated at the northern Chandeleur Islands to construct an emergency sand berm intended to mitigate island oiling from the Deepwater Horizon oil spill (Lavoie and others, 2010; Plant and others, 2014). Because the environment is similar, the same pit dimensions were used in the current study; results are only applicable for the specific potential designs evaluated with the numerical model. The proposed Breton Island restoration design is intended to mimic the island shoreline, dune platform, and back-barrier

marsh dimensions prior to Hurricane Katrina, which caused severe erosion. To accomplish this design it is estimated that a minimum of $2.3 \times 10^6 \text{ m}^3$ of sand will be required to replenish the shoreline and dune platform to pre-Katrina conditions. Some additional material may be necessary to support construction of the back-barrier marsh, which is estimated to require $550,000 \text{ m}^3$ of muddy sediments. To fully accommodate sand requirements, the size of each borrow pit was designed to provide more than $4.0 \times 10^6 \text{ m}^3$ of sediment, assuming a variable sand content of 70–100 percent and that a loss of material during excavation may occur. It is assumed that sufficient sand resources are present at each site to accommodate these excavation sand volumes. Dimensions for the borrow pits generated for the modeling scenarios are provided in table 1. For G4, the wave model was run for each of the wave scenarios for the baseline, no pit case, as well as for bathymetry grids including pit 1 and pit 2 (fig. 3).

Table 1. Dimensions of the proposed borrow pits designed for the modeling scenarios.
[m, meters]

	Water depth (m)	Pit depth ¹ (m)	Area ($\text{m}^2 \times 10^6$)	Volume ($\text{m}^3 \times 10^6$)	Volume per unit area
Pit 1	3.5 – 5.5	3.0	1.83	4.45	2.43
Pit 2	3.0 – 4.0	3.0	2.08	5.13	2.47

¹Maximum pit depth in meters below the seafloor.

Wave Impact Analysis

The primary concern if borrow pits impact patterns in wave propagation is the potential implications those changes might have on longshore sediment transport rates in the littoral system around Breton Island. In the current study, the methodology described by Adams and others (2011) was followed in which an empirical formulation was used to estimate the volumetric longshore sediment transport rate based on wave conditions. This methodology was originally proposed by Komar and Inman (1970) and later modified and named the CERC formula (Komar, 1998; Rosati and others, 2002). Even though the absolute transport values have uncertainty due to a lack of site specific calibration factors, the method has previously been used to determine relative sediment transport rates and gradients in the northern Chandeleur Islands (Georgiou and Schindler, 2009; Martinez and others, 2009). The cross-shore integrated volumetric sediment transport rate for sand-sized sediment is estimated as

$$Q_l = \frac{I_l}{(\rho_s - \rho_w)g(1 - n)} \quad (1)$$

where Q_l is volumetric sediment transport rate;
 I_l is immersed weight transport rate;
 ρ_s is density of sediment (2,650 kilograms per cubic meter);
 ρ_w is density of water (1,024 kilograms per cubic meter);
 g is gravity coefficient (9.8 meters per square second); and
 n is in-place sediment porosity (taken as 0.4).

The immersed weight transport rate is calculated by scaling the longshore component of the wave energy flux

$$I_l = KP_l \quad (2)$$

where I_l is immersed weight transport rate;

K is scaling parameter (taken as 0.8); and

P_l is longshore component of wave energy flux.

The longshore wave energy flux, as it is commonly referred to despite some objections to the terminology (Longuet-Higgins, 1972), is calculated as

$$P_l = EC_g \sin \alpha_b \cos \alpha_b = \left(\frac{1}{8} \rho_w g H_b^2 \right) \left(\frac{g H_b}{\kappa} \right)^{1/2} \sin \alpha_b \cos \alpha_b \quad (3)$$

where P_l is longshore component of wave energy flux;

E is wave energy density;

C_g is group wave celerity;

H_b is breaking wave height;

κ is breaker index (take as $1/2$); and

α_b is incident breaking wave angle relative to the shoreline.

The SWAN model outputs significant wave height (H_s), whereas H_b in the equation above is root-mean-square wave height (H_{rms}); therefore, output values of H_s were converted to H_{rms} by dividing by 1.4 (Longuet-Higgins, 1952). Alongshore flux was calculated at a set of 135 shore-normal transects at 20 m spacing along the island (fig. 4). For each scenario and transect, the breaking wave height and direction were independently found at the offshore location where the energy dissipation due to depth-induced breaking first exceeded 0.01 watt per square meter (W/m^2) as waves traveled onshore. Alongshore transport was then calculated (eqs. 1–3) at each transect. The depth and cross-shore location of incipient wave breaking was not sensitive to the choice of threshold (fig. 5). For larger energy wave cases (off-shore wave height 4+ m), the shallow slope of the inner shelf around Breton Island resulted in energy dissipation due to depth-induced breaking exceeding the 0.01 W/m^2 threshold at locations off the island platform, defined as the 4 m contour (figs. 4, 5). In these cases, the wave height and direction at 4 m water depth were used. Alongshore flux was smoothed with a 200 m filter to remove small-scale variation not well resolved at the spatial resolution of the model. Resulting values were compared between the baseline “no pit” case and the two considered borrow pit configurations.

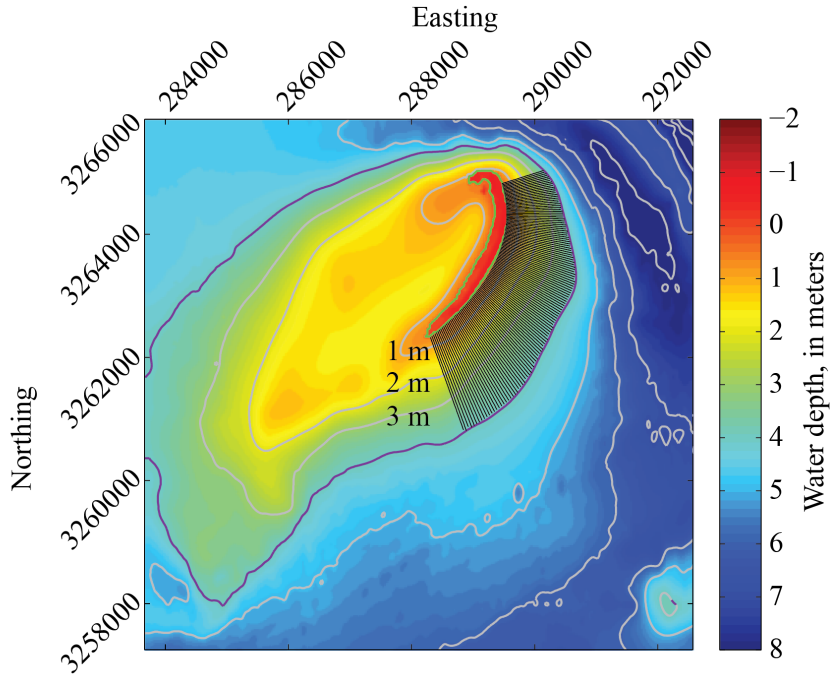


Figure 4. Portion of G4 showing the 135 cross-shore transects (in black) used in calculating the alongshore flux. Alongshore flux was calculated using wave height and direction at the most offshore point along each transect where the depth-induced wave breaking dissipation exceeded 0.01 watt per square meter. If this threshold was exceeded offshore of the island platform (defined as the 4 m contour, shown in purple), values at the 4 m contour were used instead. [m, meters]

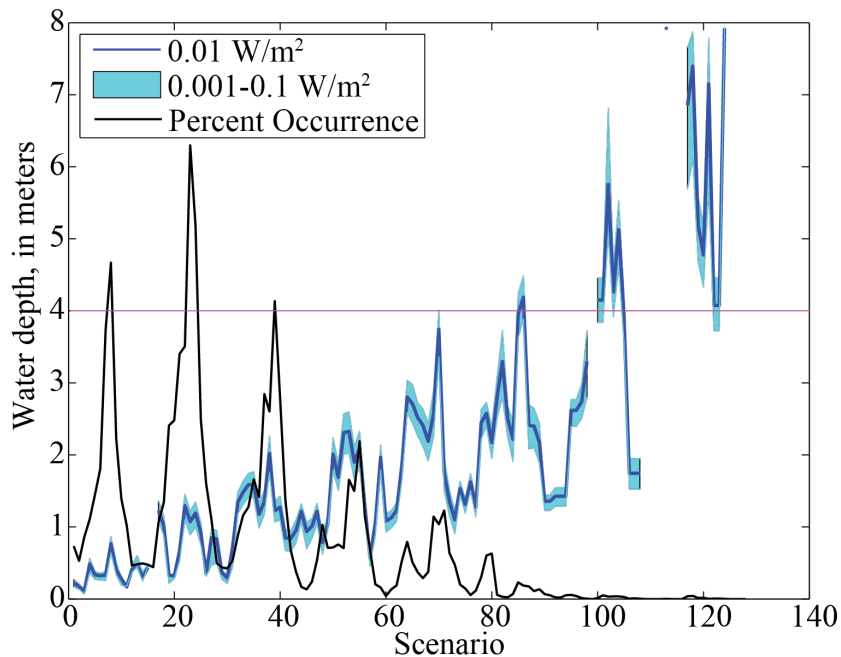


Figure 5. Depth at which depth-induced wave breaking dissipation (output from SWAN) exceeded 0.01 watt per square meter (W/m^2) (dark blue line) at 95 percent of alongshore locations for each wave scenario. Also shown are the depth at which breaking dissipation exceeded 0.001 W/m^2 and 0.1 W/m^2 (light blue band) and the percentage occurrence (black line) for each scenario. The island platform was defined as the 4 m contour (in pink; fig. 4), and in cases where the threshold of breaking dissipation was exceeded at deeper than 4 m, values from this depth were used in calculating alongshore flux.

The focus of the work was to examine changes in wave propagation and wave-breaking induced longshore sand-sized sediment transport near the island. Hence, no account was made for sediment input from the adjacent Mississippi River plume, which brings fine-grained sediment to the inner shelf and beyond. The effect of tidal currents around the island was also not considered due to the microtidal range of 30 centimeters (cm) (Boyd and Penland, 1988). These processes have likely contributed to the shape of the underlying island platform, but are expected to have less influence on shoreline evolution than the wave-induced transport of sand-sized sediment estimated by equations 1–3. Model results can only be used to infer the potential effects of the specific borrow pit designs considered on longshore transport. Analysis did not include assessments of cross-shore sediment transport or island overwash and inundation processes that also affect the short- and long-term topology and morphology of the island and island platform but are not expected to be affected by the dredging of borrow pits.

Results

An accurate assessment of the effects of proposed borrow pits on inshore wave climatology relies on the skill of the scenario-based wave modeling approach in predicting the nearshore wave field. A comparison of wave model results to observations at buoys within the model domains for grids G1 and G2 are described in the section “Numerical Model Assessment;” grids G3 and G4 did not encompass buoys to be used for comparison. Included are (1) a comparison of the shallower wave buoy observations to numerical model results, evaluating the ability of the model to represent the spatial transformation of waves, and (2) the accuracy of a scenario-based wave reconstruction for all available buoy times, indicating the ability of the scenario-based approach to capture wave climate at any given time. The results of tests to determine the need to include triad interactions and wave diffraction in the model are described in the section “Sensitivity Analysis.” Finally, analysis of the effects of the proposed wave borrow pit designs on the wave climate around Breton Island is presented in “Effects of Borrow Pits on Nearshore Wave Climate and Longshore Transport.”

Numerical Model Assessment

Data from three NDBC directional wave buoys (42040, 42012, and 42007; fig. 1) were used to assess model output (significant wave height, wave period, and wave direction) for each of the 116 different scenarios for G1 and G2. For G1 (fig. 6), all three buoys were used to compare model outputs for each of the 116 scenarios, whereas for G2 (fig. 7), only buoys 42012 and 42007 were within the bounds of the grid domain. The comparison of wave characteristics to observations at the buoys for the representative times for each scenario assesses the ability of the wave model to propagate waves inshore (for buoys 42012 and 42007) and assesses the accuracy of boundary conditions for buoy 42040. The ability of the G1 and G2 models to predict observations is comparable to the ability of the operational WavewatchIII® model (table 2).

The ability of WavewatchIII® to simulate wave conditions at buoy 42040, which lies just inside the boundary of G1, is acceptable for wave height, period, and direction, illustrating that the WavewatchIII® model resolves wave height conditions sufficiently to provide boundary conditions for SWAN G1 (table 2; fig. 6). The accuracy and precision of WavewatchIII®, however, decreases moving into shallower water, exhibiting higher magnitude bias, much lower values of squared-correlation coefficient (R^2), and higher root-mean square error (RMSE). In contrast, the G1 (fig. 6) and G2 (fig. 7) grids retain lower magnitude bias and RMSE and higher values of R^2 moving into shallower water. The improved predictions are possibly a result of the finer spatial resolution of G1 and G2 (1,500 m and 300 m,

respectively, compared to a spatial resolution for WavewatchIII® of ~ 7.5 km) or better ability of SWAN to resolve shallow water and nearshore wave transformation processes than WavewatchIII®. There is little difference in the RMSE and R^2 values for buoys 42012 and 42007 in G2 compared to G1 (table 2).

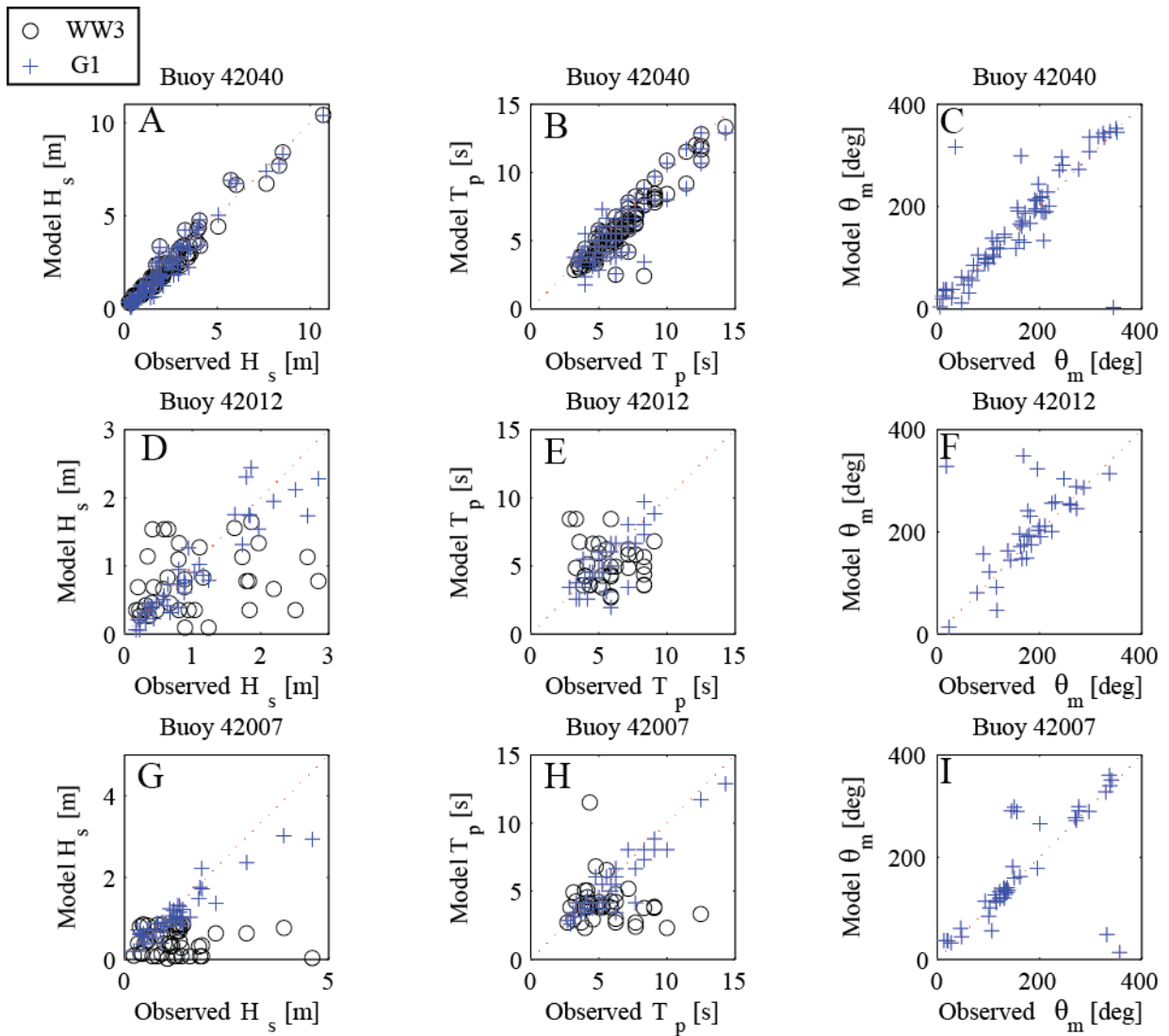


Figure 6. Comparison of the Simulating WAVes Nearshore (SWAN) grid G1 and WavewatchIII® model output of significant wave height (A,D,G), peak wave period (B,E,H), and mean wave direction (C,F,I) versus observations at National Data Buoy Center (NDBC) buoys 42040, 42012, and 42007. Operational WavewatchIII® does not archive mean direction, so this variable cannot be assessed. G1 has a spatial resolution of approximately 500 m and encompasses the northern Gulf of Mexico. The spatial extent of the grid and location of the buoys used for model assessment are shown in figure 1. [m, meters; s, seconds; deg, degrees]

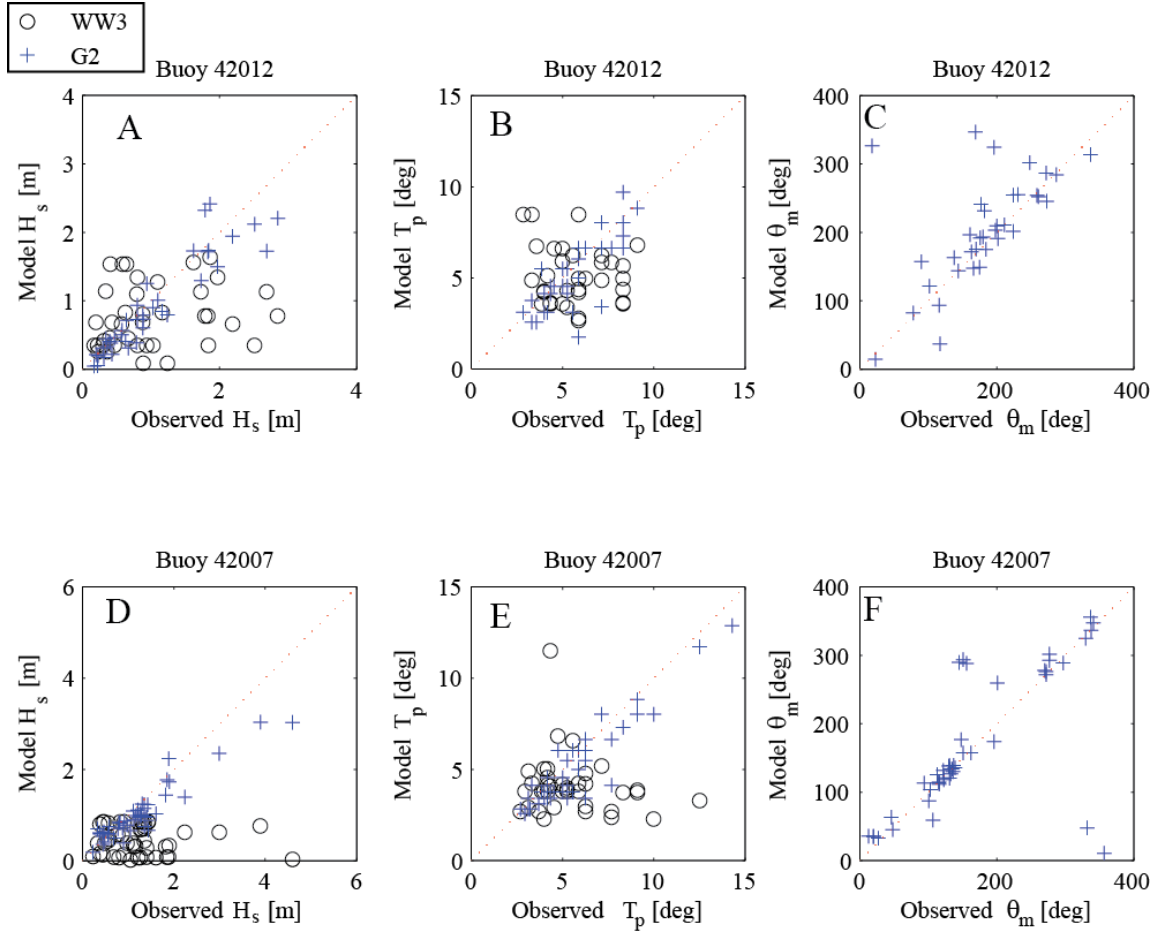


Figure 7. Comparison of Simulating WAVes Nearshore (SWAN) and WavewatchIII® G2 model output of significant wave height (A,D), peak wave period (B,E), and mean wave direction (C,F) versus observations at National Data Buoy Center (NDBC) buoys 42012 and 42007 for each scenario. Operational WavewatchIII® does not archive mean direction, so this variable cannot be assessed. G2 has a spatial resolution of approximately 300 m and encompasses the western half of the northern Gulf of Mexico. The spatial extent of the grid and location of the buoys used for model assessment are shown in figure 1. [m, meters; deg, degrees]

Table 2. Comparison of the Simulating WAVes Nearshore (SWAN) model output from grids G1 and G2 to WavewatchIII® model output evaluated against observed buoy data from the representative time step of each scenario. Operational WavewatchIII® does not archive mean direction, so this variable cannot be assessed.

[m, meters; R², coefficient of determination; RMSE, root-mean square error; s, seconds; --, indicates no error calculated for buoy observations]

Buoy	Depth (m)	Significant wave height (m)				Peak wave period (s)				Mean wave direction (degree)			
		Mean	Bias	RMSE	R ²	Mean	Bias	RMSE	R ²	Mean	Bias	RMSE	R ²
Observed													
42040	164.6	2.46	--	--	--	6.92	--	--	--	134.4	--	--	--
42012	27.7	1.1	--	--	--	5.77	--	--	--	189.5	--	--	--
42007	14.9	1.46	--	--	--	5.88	--	--	--	117.6	--	--	--
WaveWatch III													
42040	164.6	2.36	-0.1	0.42	0.96	6.15	-0.77	0.85	0.87	--	--	--	--
42012	27.7	0.77	-0.33	0.44	0.05	5.1	-0.67	1.51	0.02	--	--	--	--
42007	14.9	0.48	-0.98	0.31	0.01	4.12	-1.77	1.46	0.05	--	--	--	--

Table 2. Comparison of the Simulating WAVes Nearshore (SWAN) model output from grids G1 and G2 to WavewatchIII® model output evaluated against observed buoy data from the representative time step of each scenario. Operational WavewatchIII® does not archive mean direction, so this variable cannot be assessed.—Continued

[m, meters; R², coefficient of determination; RMSE, root-mean square error; s, seconds; --, indicates no error calculated for buoy observations]

Buoy	Depth (m)	Significant wave height (m)				Peak wave period (s)				Mean wave direction (degree)			
		Mean	Bias	RMSE	R ²	Mean	Bias	RMSE	R ²	Mean	Bias	RMSE	R ²
SWAN G1													
42040	164.6	2.36	-0.11	0.52	0.95	6.25	-0.67	0.98	0.83	119.8	5	27.43	0.93
42012	27.7	0.97	-0.13	0.25	0.87	5.42	-0.35	1.15	0.64	216.3	11.87	44.85	0.72
42007	14.9	1.21	-0.25	0.24	0.93	5.37	-0.52	0.83	0.88	84.49	16.41	38.66	0.87
SWAN G2													
42012	27.7	0.95	-0.15	0.25	0.87	5.37	-0.4	1.15	0.64	216.4	11.37	45.14	0.72
42007	14.9	1.18	-0.29	0.25	0.92	5.28	-0.6	0.87	0.87	86.32	15.99	38.08	0.87

Continuous time series of wave characteristics (height, period, and direction) were constructed at NDBC buoys 42012 (fig. 8) and 42007 (fig. 9) on the basis of probabilistic methods from Long and others (2014). The probabilistic method used offshore buoy observations at NDBC buoy 42040 to identify which of the 116 scenarios was the best match to each time step in the observed record. Time series of wave characteristics were then reconstructed for comparison to observations by extracting G2 model results at the locations of buoys 42012 and 42007 and ordering them on the basis of the sequence of best match scenarios. The accuracy of the time series reconstructions evaluated the ability of the scenario-based approach to capture the full local wave climatology and variability, in addition to the ability of the model to capture spatially variant wave transformation processes within the domain (previously evaluated in the assessment of model accuracy for the representative time steps, as discussed previously). Model assessment included bias, linear regression slope, RMSE, R², and the model skill (*S*) defined (Gallagher and others, 1998; Reniers and others, 2004) as

$$S = 1 - \frac{\sqrt{\frac{1}{N} \sum_{i=1}^N (\alpha_{o,i} - \alpha_{m,i})^2}}{\sqrt{\frac{1}{N} \sum_{i=1}^N \alpha_{o,i}^2}} \quad (4)$$

where *S* is model skill score;
N is number of observations;
 α_o is observed values; and
 α_m is predicted values.

A summary of these statistical results is presented in table 3. A value of *S* = 1 indicates perfect model-data agreement. Model skill is dependent on the ratio between the standard deviation in model-data mismatch and the standard deviation in the data; skill increases when the standard deviation of the data is large compared to the mismatch.

The bias for significant wave height at buoys 42012 and 42007 was low at 3 cm and 5 cm, with an R² of 0.70 and 0.37, respectively (table 3). Model skill, *S*, was 0.70 and 0.5 for 42012 and 42007, respectively. Bias for peak wave period for both buoys was low (~0.2 s), R² values were lower for peak

wave period (~ 0.2) than for wave height, and the skill score improved (0.73 and 0.67). For mean wave direction, the bias was 3.31 degrees for 42012 and double that (7.67) for 42007, with model skill values similar to peak wave period and somewhat higher R^2 values (0.58 and 0.55, respectively).

The transformation of waves from the offshore buoy (42040) to the inshore buoys (42012 and 42007) was effectively captured by the reconstruction (figs. 8 and 9). In addition, when winds were blowing from the north, the reconstruction predicted the smaller waves observed at the inshore buoys as a result of short fetch distance between the coastline and the location of observations despite larger measured offshore wave heights. The majority of wave height predictions (height, period, and direction) fall along a 1:1 line with observations (figs. 10 and 11), and accuracy in predicting larger wave heights was improved relative to a previous application of the scenario-based approach by increasing the number of bins for wave heights greater than 2 m (see Long and others, 2014).

The primary concern with the reconstruction application was whether wave characteristics were modeled accurately enough to create robust predictions of alongshore transport. Alternate approaches to predicting nearshore wave conditions are (1) deploying an array of instruments and (2) running a deterministic, time-variant model. Both strategies have the inherent problem of typically capturing a shorter record of time (due to cost or computational expense) than is needed to fully capture the wave climatology; however, comparing the accuracy of the scenario-based model against a deterministic approach is useful for benchmarking it against a commonly used strategy for predicting waves. The model assessment indicates that the probabilistic reconstruction method was able to resolve wave characteristics at least as effectively as the deterministic model Wavewatch III®, while eliminating a bias observed in WavewatchIII® at higher wave periods at buoy 42012. Comparing tables 2 and 3 indicates that the error in wave predictions is similar between the direct simulations (table 2) and the probabilistic reconstruction (table 3). These results indicate that the probabilistic reconstruction used for the assessment is capable of providing results with accuracy similar to assessments that use deterministic model simulations. A previous assessment of the wave climatology approach (Long and others, 2014) also found this approach as accurate as both a Bayesian approach to transforming waves between two locations with historical observations to train the model and a deterministic model run on the same numerical model domain, the latter approach of which is often employed in modeling borrow pit effects on wave climatology (for example, Benedet and List, 2008; Adams and others, 2011).

Table 3. Reconstruction performance and error statistics using the 116 unique scenarios generated for grid G2.

[m, meters; H_s , significant wave height; T_p , peak wave period; Θ , mean wave direction; R^2 , coefficient of determination; RMSE, root-mean square error]

		Buoy 42012 (30 m)	Buoy 42007 (15 m)
Observed mean	$H_s[m]$	0.76	0.68
	$T_p[s]$	5.29	5.05
	$\Theta[deg]$	156.9	122.4
Reconstructed mean	$H_s[m]$	0.81	0.64
	$T_p[s]$	5.12	4.82
	$\Theta[deg]$	156.5	131.1
RBias	$H_s[m]$	-0.03	-0.05
	$T_p[s]$	-0.28	-0.23
	$\Theta[deg]$	-3.31	7.67

Table 3. Reconstruction performance and error statistics using the 116 unique scenarios generated for grid G2.—Continued
 [m, meters; H_s , significant wave height; T_p , peak wave period; Θ , mean wave direction; R^2 , coefficient of determination; RMSE, root-mean square error]

		Buoy 42012 (30 m)	Buoy 42007 (15 m)
RMSE	$H_s[m]$	0.26	0.42
	$T_p[s]$	1.50	1.75
	$\Theta[deg]$	44.7	56.7
Slope	H_s	0.88	0.85
	T_p	0.48	0.54
	Θ	0.87	0.92
R^2	H_s	0.70	0.37
	T_p	0.22	0.28
	Θ	0.58	0.55
Skill	H_s	0.70	0.50
	T_p	0.73	0.67
	Θ	0.75	0.65

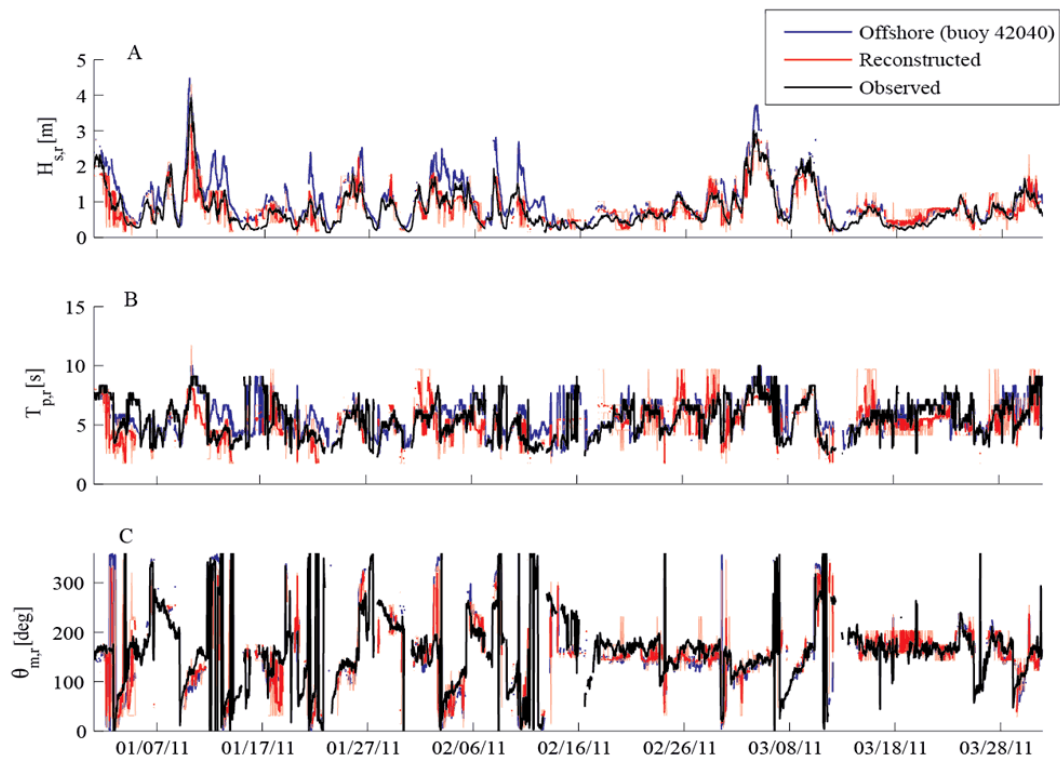


Figure 8. Time series above shows a portion (January 1, 2011, through March 31, 2011) of the entire probabilistic wave reconstructed time series (August 24, 2000, to January 31, 2013) at buoy 42012 comparing the observations (black), reconstructed values (red; Long and others, 2014), and measurement at offshore buoy 42040 (blue). [m, meters; s, seconds; deg, degrees]

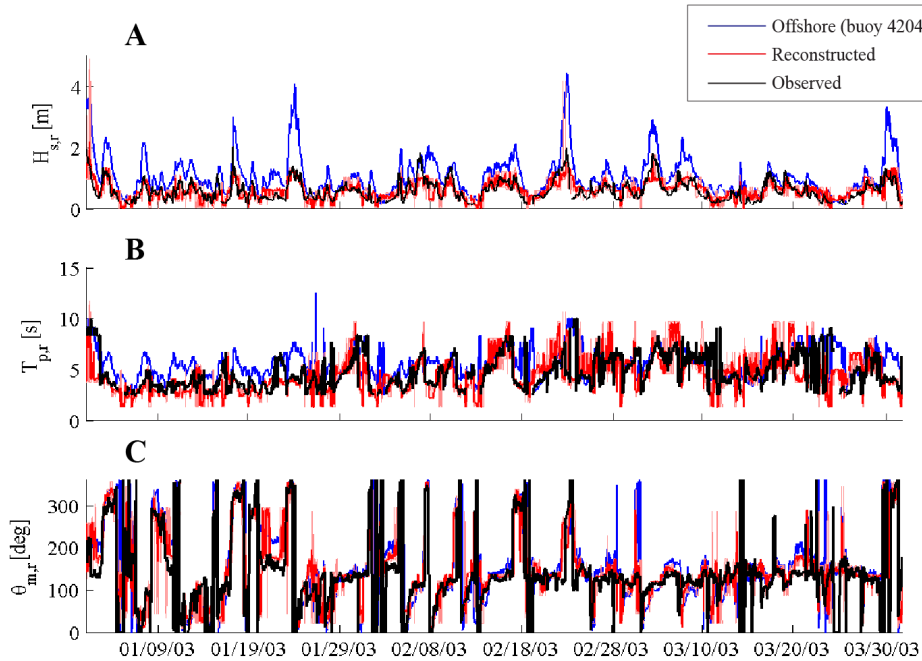


Figure 9. Time series above shows a portion (January 1, 2003, through March 31, 2003) of the entire probabilistic wave reconstructed time series (December 4, 1995, to December 30, 2013) at buoy 42007 comparing the observations (black), constructed values (red; Long and others, 2014), and measurement at offshore buoy 42040 (blue). [m, meters; s, seconds; deg, degrees]

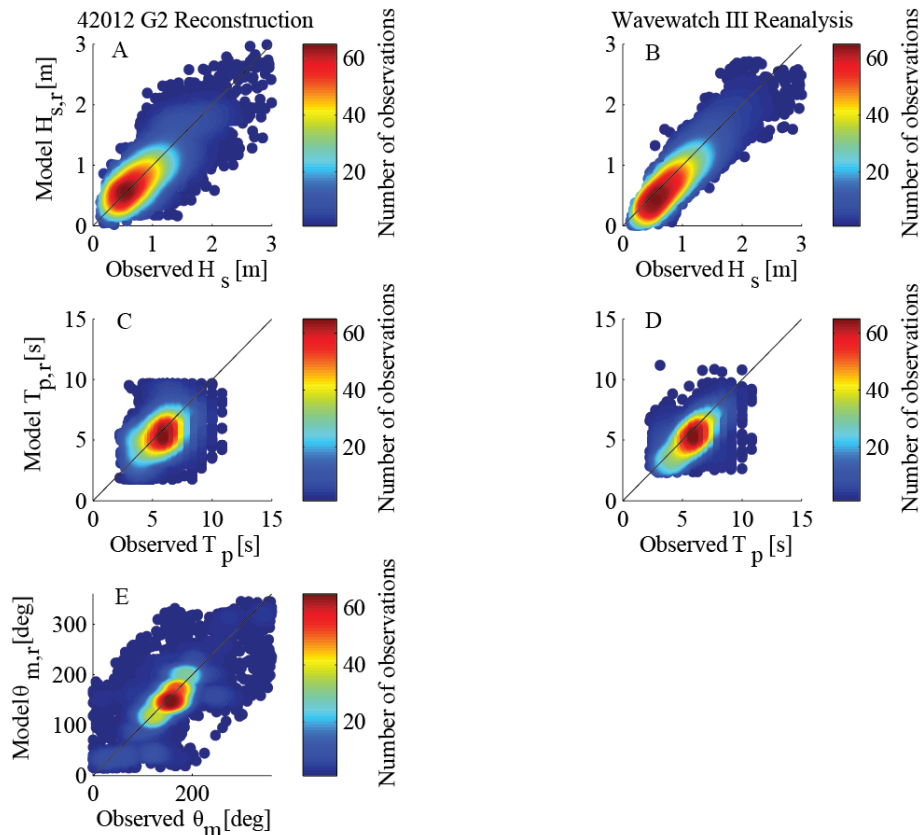


Figure 10. Comparison of wave time series constructed using probabilistic method and observations at National Data Buoy Center (NDBC) buoy 42012 for April 2, 2010, to December 30, 2013, (left column) and comparison of the WavewatchIII® dataset and the observations for the same time period (right column). Comparisons of (A, B) significant wave height, (C, D) peak wave period, and (E) mean wave direction. WavewatchIII® output is every 3 hours, whereas Simulating WAVes Nearshore (SWAN) results are hourly, resulting in a larger number of points. [m, meters; s, seconds; deg, degrees]

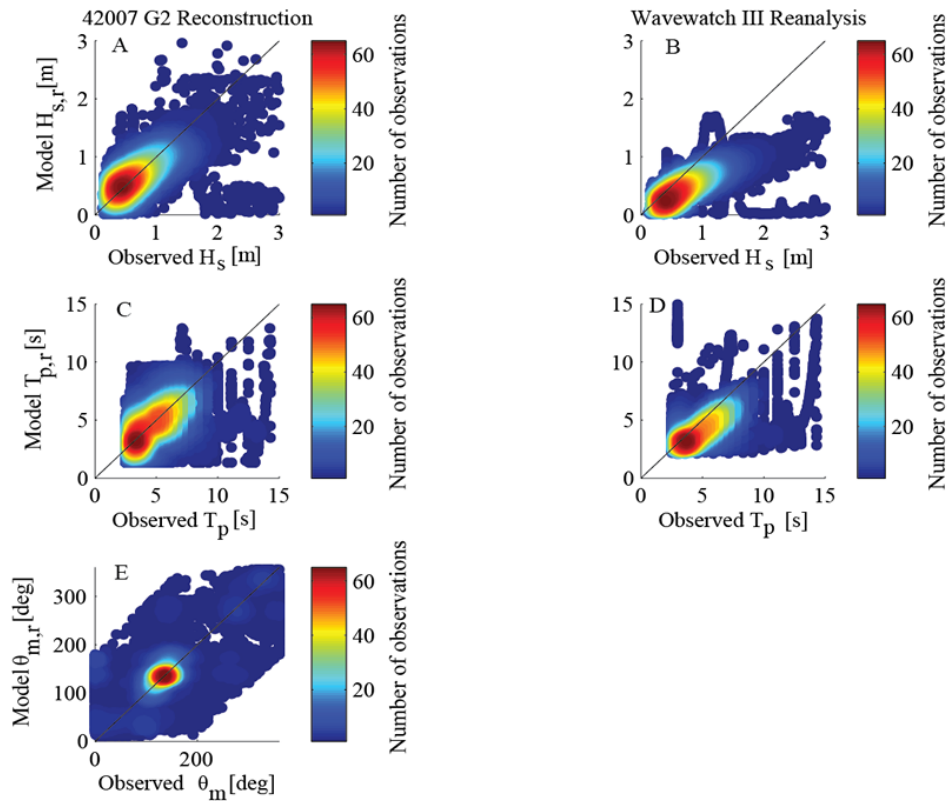


Figure 11. Comparison of wave time series constructed using probabilistic method and observations at NDBC buoy 42007 for the time period January 19, 2005, to February 15, 2008, (left column) and comparison of the WavewatchIII® dataset and the observations for the same time period (right column). Comparisons of (A, B) significant wave height, (C, D) peak wave period, and (E) mean wave direction. WavewatchIII® output is every 3 hours, whereas Simulating WAves Nearshore (SWAN) results are hourly, resulting in a larger number of points. [m, meters; s, seconds; deg, degrees]

Sensitivity Analysis

Sensitivity tests were performed on grids G3 and G4 to determine the effect of triad wave-wave interactions and wave diffraction on the wave model predictions when a borrow pit was present (pit 1 used for comparisons). Comparison of model scenarios with diffraction turned on versus off in the SWAN model showed minimal change (less than 1 cm) in significant wave height (fig. 12), and thus diffraction was not included in runs analyzing borrow pit impact. Triad wave interactions are relevant to shallow water wave transformation, and sensitivity testing was undertaken to determine triad effects on the G3 and G4 grids. Triads did prove to alter the wave model output enough (~10 cm) (fig. 13) to prompt use of these wave interactions in all of the G3 and G4 modeled scenarios. In particular, wave heights near Breton Island were reduced with the inclusion of triads, possibly as a result of greater dissipation due to bottom friction of the higher frequency (longer period) waves that were generated. Note, one other possible explanation would be that SWAN integration of energy to calculate wave height excluded the higher frequencies generated through triad interactions; however, the version of SWAN used (41.01) integrates over the entire range of user-defined frequencies, which at 0.04–1 Hertz includes the range of frequencies expected to be generated through triads (Herbers and others, 2000).

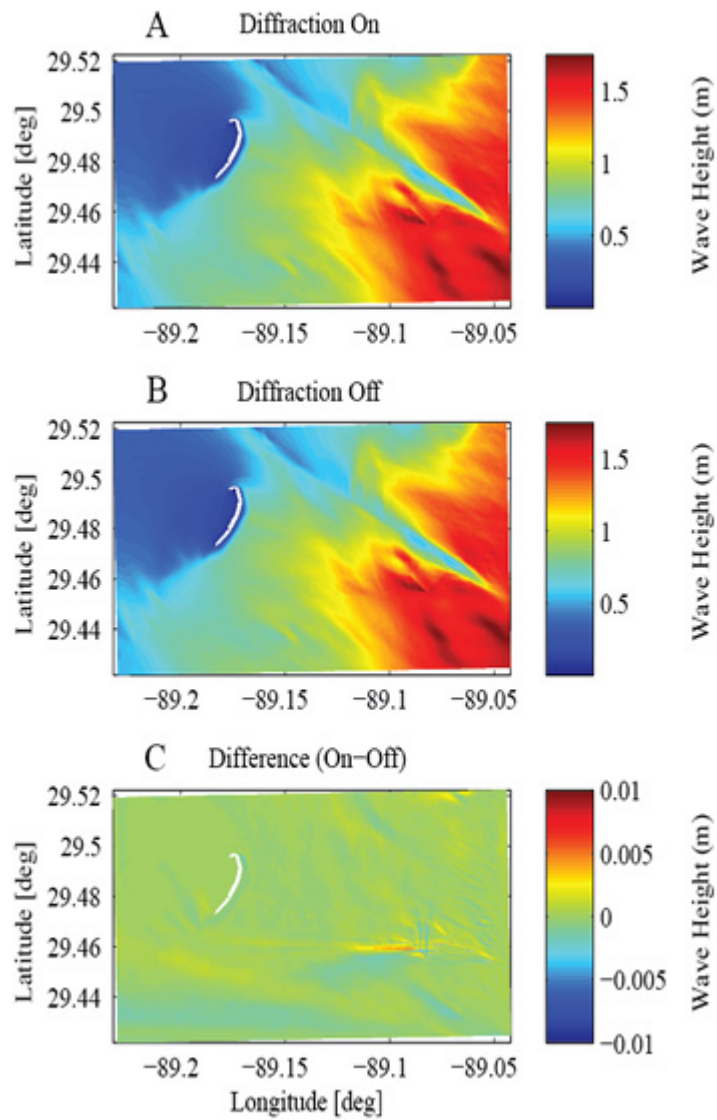


Figure 12. Model sensitivity to wave diffraction in grid G4 with pit 1 present for scenario H6_D7. (A) Significant wave height (in meters) results with diffraction on, (B) Significant wave height results with diffraction off, (On minus Off), difference in significant wave height from both results. [deg, degrees; m, meters]

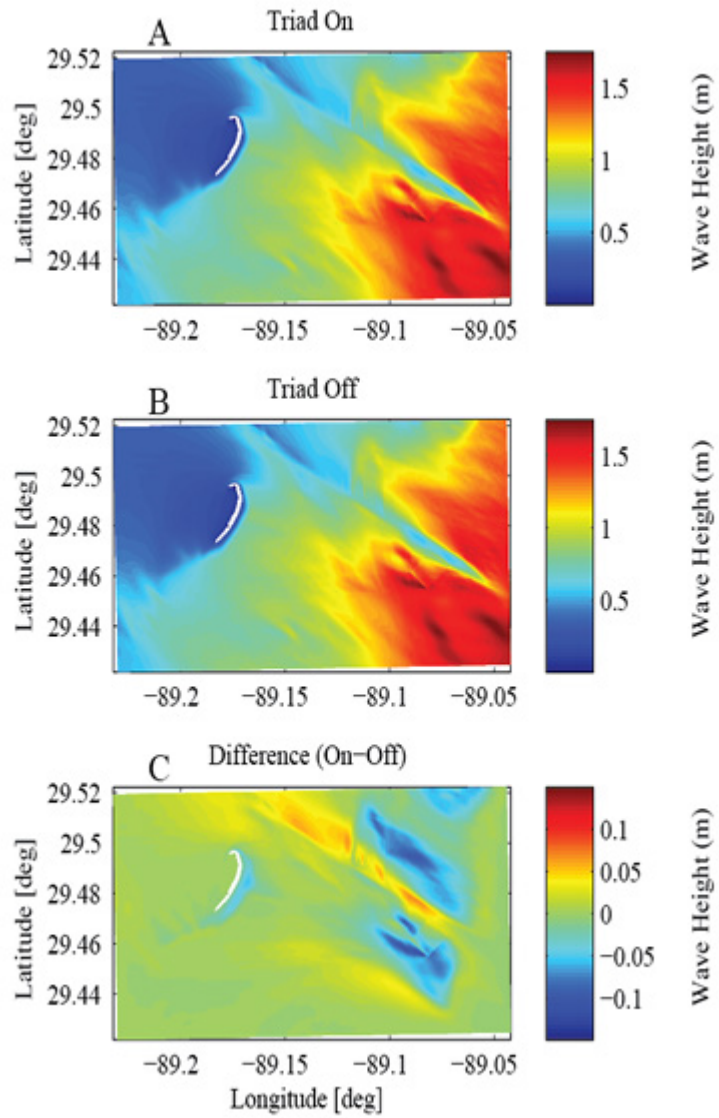


Figure 13. Model sensitivity to wave triads in grid G4 with pit 1 present for scenario H6_D7. Significant wave height (in meters) results with triads on (A), significant wave height results with triads off (B), difference in significant wave height from both results (On minus Off). [deg, degrees; m, meters]

Effects of Borrow Pits on Nearshore Wave Climate and Longshore Transport

The effect of the proposed borrow pits on the wave climate around Breton Island was first assessed by calculating a weighted average wave height over the model domain for the baseline (no pit), pit 1, and pit 2 configurations. To compute this composite wave height distribution, the wave height results for each scenario were weighted by the frequency of occurrence from the wave climatology (fig. 2). Comparing the weighted average wave height for the three configurations showed that the wave climate was only noticeably modified in the immediate vicinity of the borrow pit, resulting in a slight shadowing effect originating from the western corners of each pit (fig. 14). The magnitude of the change in weighted average wave height was less than 10 cm, or 5 percent of the baseline wave height, with no discernable change in wave height extending to the nearshore contours around Breton Island. The maximum change in significant wave height for a single scenario was an increase of 74 cm, occurring on the northeast side of borrow pit 1 (fig. 3) for scenario H8_D1 (fig. 2) when the wave conditions in the baseline case at that location were 1.6 m.

The longshore transport rate (LSTR) around Breton Island varied by wave scenario, with the largest transport rates associated with larger offshore wave heights (fig. 15; no pit case). Transport magnitude and direction also varied alongshore with incident wave direction.

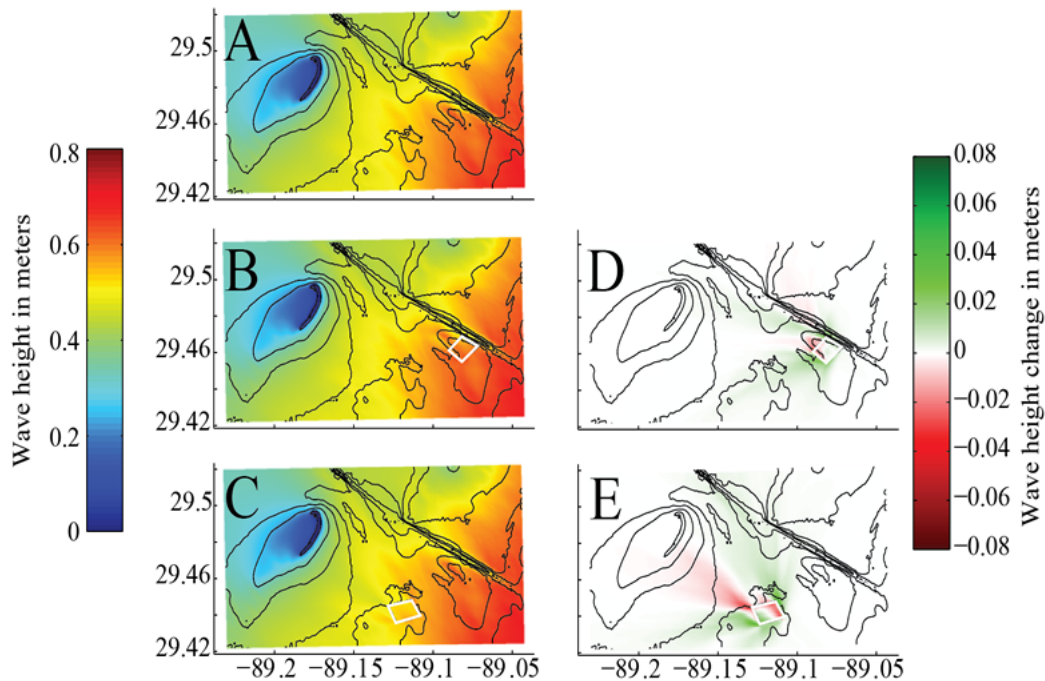


Figure 14. Weighted average significant wave height for the (A) baseline, no pit bathymetry, (B) bathymetry including borrow pit 1 (change from baseline shown in D), and (C) bathymetry including borrow pit 2 (change from baseline shown in E). Borrow pits are outlined in white. The average is created from the output of individual scenarios, weighted by their percentage occurrence over the time period December 1995 through December 2013 (fig. 2). The pits create a shadowing effect originating from the corners.

The LSTR with the addition of the borrow pits (fig. 16) was similar to the LSTR without the pits, with a change of less than 0.004 cubic meters per second (m^3/s) (approximately 10 percent of the magnitude of the baseline condition without borrow pits).

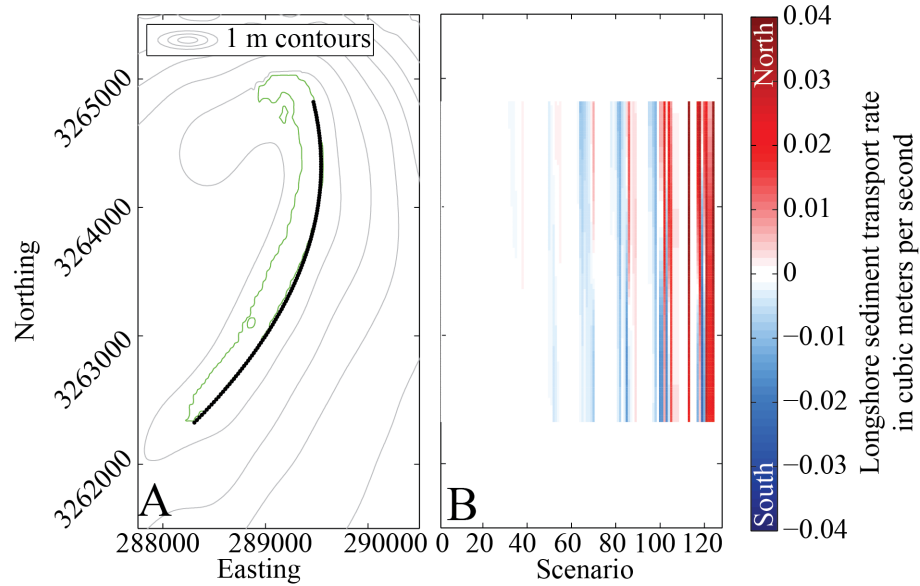


Figure 15. For 135 locations (A, black line) along Breton Island (0 m contour shown in green), longshore transport rate (B; eq. 1) for each of the 116 wave scenarios (fig. 2) for the no pit case. Red colors indicate northerly transport and blue colors indicate southerly transport. Moving from left to right in (B), the magnitude of transport increases for larger wave scenarios. Because the dominant wave direction for storms is from the south and southeast (fig. 2), there are few large wave scenarios with predominantly southerly directed transport. [m, meters]

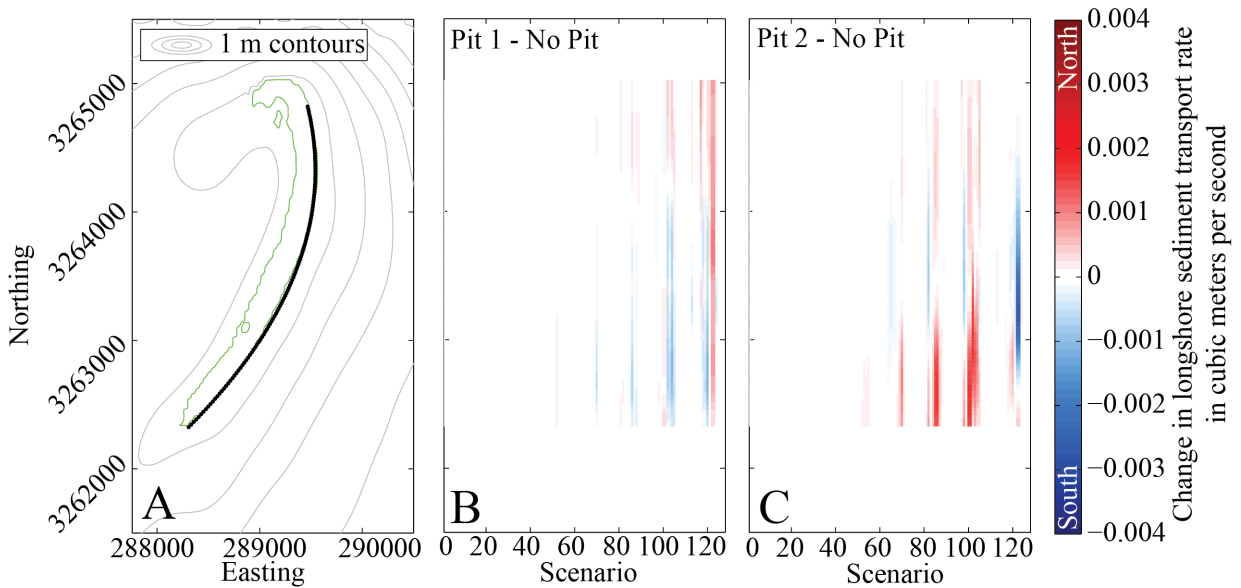


Figure 16. For 135 locations (A, black line) along Breton Island (0 m contour shown in green), change in the longshore transport rate (eq. 1) with the addition of pit 1 (B) and pit 2 (C) for each of the 116 wave scenarios (fig. 2). Red colors indicate a positive change in transport (more northerly or less southerly) and blue colors indicate negative change transport (more southerly or less northerly).

Changes in the transport were also assessed by calculating the alongshore variant average LSTR (fig. 17) weighted by the frequency of occurrence of the 116 wave climatology scenarios (fig. 2). The shape of the alongshore variant LSTR curve did not change with the addition of the borrow pits, and the change in transport magnitude was an order of magnitude less than the baseline case.

Also considered were changes in the gradient of alongshore variant average LSTR (fig. 18). In all cases (pits and no pit), the model predicted accretion at the northern and southern ends and erosion in the center of the island arc. Changes in the gradient of transport were an order of magnitude less than the gradient for the no pit case. The overall shape of the gradient in LSTR did not change with the addition of the pits, and no new convergences or divergences were identified that would potentially be associated with the formation of accretional or erosional “hot spots.” In the case of pit 2 (fig. 1), the magnitude of erosion would be expected to decrease slightly in a region toward the southern end of the island (fig. 17), with slightly more erosion to the north and slightly less accretion to the south of that stretch of island.

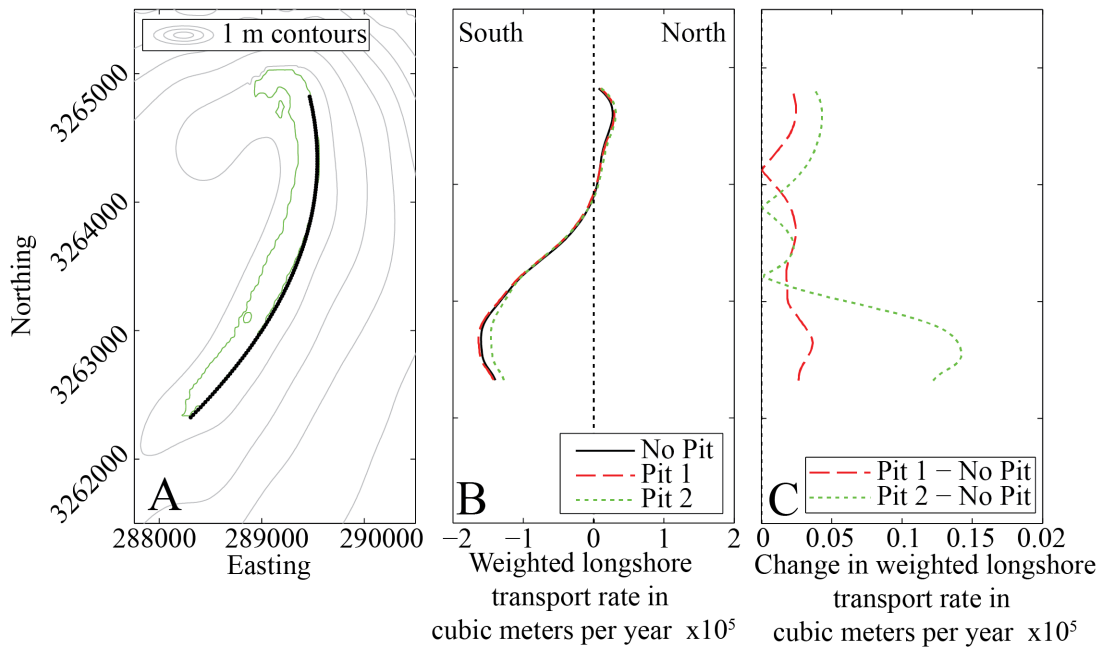


Figure 17. For 135 locations (A, black line) along Breton Island (0 m contour shown in green), gradient of average longshore transport rate (B, LSTR) calculated by weighting each of the 116 individual scenario results by its frequency of occurrence in the wave climatology (fig. 2). The change in magnitude of the weighted average longshore transport rate (C) with the addition of the pits is an order of magnitude less than the baseline values, and the overall pattern in transport is the same (B).

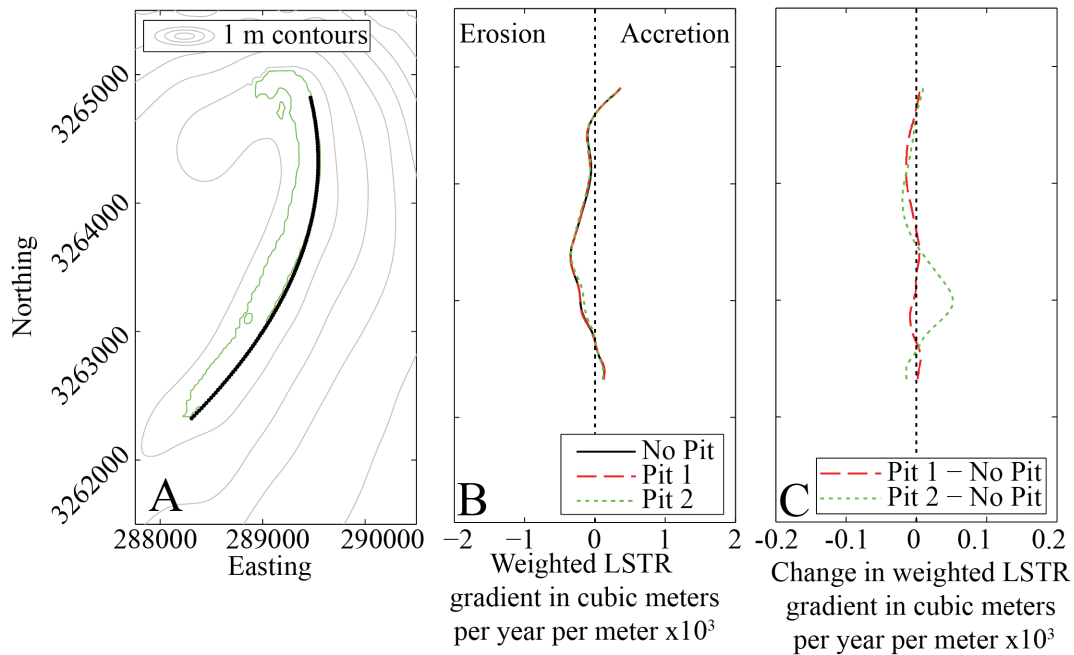


Figure 18. Gradient of average longshore transport rate (B, LSTR) constructed from the longshore transport calculated using wave conditions at 135 locations (A, black line) along Breton Island (0 m contour shown in green) for each of the 116 individual scenario results (e.g., fig. 15 for the no pit case) by weighting each scenario by its frequency of occurrence in the wave climatology (fig. 2). The change in magnitude of the gradient of the LSTR (C) with the addition of the pits is an order of magnitude less than the baseline values, and the overall pattern in transport is the same (B). Positive values in (C) indicate more accretion or less erosion, negative values indicate less accretion or more erosion.

Conclusions

A numerical wave model was developed to study the potential impact of proposed sediment borrow pits on the wave characteristics and longshore sediment transport rate (LSTR) near Breton Island, Louisiana. The model consisted of four nested domains that were used to simulate a set of 116 scenarios derived from a wave climatology for a baseline (no pit) condition and two proposed borrow pit configurations. Surf zone wave characteristics for each scenario provided the input for an empirical model for the LSTR. Model results for bathymetries including the proposed pits were compared to the baseline case to determine the impact the particular borrow pit designs considered would have on wave climatology and alongshore transport at Breton Island.

Comparisons between the wave height predicted for the baseline case and the two borrow pit configurations showed that changes in significant wave height were less than 10 centimeters and largest in the immediate vicinity of the borrow pit. The LSTR direction and magnitude depended on the individual wave scenario. The change in magnitude of the calculated LSTR with the addition of the two borrow pits was an order of magnitude less than the LSTR calculated for the baseline case. The gradient of LSTR changed somewhat with the addition of the borrow pits, particularly in a region of slightly less erosion toward the southern end of the island, with slightly more erosion to the north and slightly less accretion to the south of that location; however, changes were less than an order of magnitude of the baseline gradient with no pits, and no new convergences or divergences of sediment transport were identified.

Acknowledgments

This research was chartered by the U.S. Fish and Wildlife Service.

References Cited

- Adams, P.N., Inman, D.L., and Lovering, J.L., 2011, Effects of climate change and wave direction on longshore sediment transport patterns in Southern California: *Climatic Change*, v. 109, p. S211–S228.
- Battjes, J.A., and Janssen, J.P.F.M., 1978, Energy loss and set-up due to breaking of random waves, chap. 32 of *Coastal engineering—1978: Conference on Coastal Engineering*, 16th, Hamburg, Germany, Proceedings, p. 569–587.
- Bender, C.J., and Dean, R.G., 2003, Wave field modification by bathymetric anomalies and resulting shoreline changes—A review with recent results: *Coastal Engineering*, v. 49, no. 1–2, p. 125–153.
- Benedet, L., Finkl, C.W., and Dobrochinski, J., 2013, Optimization of nearshore dredge pit design to reduce impacts on adjacent beaches: *Journal of Coastal Research*, v. 29, no. 3, p. 519–525.
- Benedet, L., Finkl, C.W., and Hartog, W.M., 2007, Processes controlling development of erosional hot spots on a beach nourishment project: *Journal of Coastal Research*, v. 23, no. 1, p. 33–48.
- Benedet, L., and List, J., 2008, Evaluation of the physical process controlling beach changes adjacent to nearshore dredge pits: *Coastal Engineering*, v. 55, no. 12, p. 1224–1236.
- Booij, N., Ris, R.C., and Holthuijsen, L.H., 1999, A third-generation wave model for coastal regions—1. Model description and validation: *Journal of Geophysical Research*, v. 104, no. C4, p. 7649–7666.
- Boyd, R., and Penland, S., 1988, A geomorphologic model for Mississippi Delta evolution: *Gulf Coast Association of Geological Societies Transactions*, v. 38, p. 443–452.
- Byrnes, M.R., Hammer, R.M., Thibaut, T.D., and Snyder, D.B., 2004, Physical and biological effects of sand mining offshore Alabama, U.S.A.: *Journal of Coastal Research*, v. 20, no. 1, p. 6–24.
- Combe, A.J., III, and Soileau, C.W., 1987, Behavior of man-made beach and dune, Grand Isle, Louisiana: *Coastal Sediments '87*, p. 1233–1242.
- Demir, H., Otay, E., Work, P., and Bőreckçi, O., 2004, Impacts of dredging on shoreline change: *Journal of Waterway, Port, Coastal, and Ocean Engineering*, v. 130, no. 4, p. 170–178.
- Flocks, J., Twichell, D., Sanford, J., Pendleton, E., and Baldwin, W., 2009, Sediment sampling analysis to define quality of sand resources, chap. F, in Lavoie, D., ed., *Sand resources, regional geology, and coastal processes of the Chandeleur Islands coastal system—An evaluation of the Breton National Wildlife Refuge*: U.S. Geological Survey Scientific Investigations Report 2009–5252, p. 99–124.
- Gallagher, E.L., Elgar, S., and Guza, R.T., 1998, Observations of sand bar evolution on a natural beach: *Journal of Geophysical Research*, v. 103, no. C2, p. 3203–3215.
- Georgiou, I.Y., and Schindler, J.K., 2009, Wave forecasting and longshore sediment transport gradients along a transgressive barrier island—Chandeleur Islands, Louisiana: *Geo-Marine Letters*, v. 29, p. 467–476.

- Gonçalves, D., Pinheiro, L., Silva, P., Rosa, J., Rebêlo, L., Bertin, X., Teixeira, S. B., and Esteves, R., 2014, Morphodynamic evolution of a sand extraction excavation offshore Vale do Lobo, Algarve, Portugal: *Coastal Engineering*, v. 88, p. 75–87.
- Hartog, W.M., Benedet, L., Walstra, D.-J.R., van Koningsveld, M., Stive, M.J.F., and Finkl, C.W., 2008, Mechanisms that influence the performance of beach nourishment: A case study in Delray Beach, Florida, U.S.A.: *Journal of Coastal Research*, v. 24, no. 5, p. 1304–1319.
- Hasselmann, K., Barnett, T.P., Bouws, E., Carlson, H., Cartwright, D.E., Enke, K., Ewing, J.A., Gienapp, H., Hassellman, D.E., Kruseman, P., Meerburg, A., Müller, P., Olbers, D.J., Richter, K., Sell, W., and Walden, H., 1973, Measurements of wind-wave growth and swell decay during the Joint North Sea Wave Project (JONSWAP): Hamburg, Germany, *Deutsches Hydrographisches Institut Ergänzungsheft zur Deutschen Hydrographischen Zeitschrift Reihe A*, v. 8, no. 12, 95 p.
- Herbers, T.H.C., Russnogle, N.R., and Elgar, S., 2000, Spectral energy balance of breaking waves within the surf zone: *Journal of Physical Oceanography*, v. 30, no. 11, p. 2723–2737.
- Kennedy, A.B., Slatton, K.C., Starek, M., Kampa, K., and Cho, H.-C., 2009, Hurricane response of nearshore borrow pits from airborne bathymetric lidar: *Journal of Waterway, Port, Coastal, and Ocean engineering*, v. 136, no. 1, p. 46–58.
- Komar, P.D., 1998, *Beach processes and sedimentation* (2d ed.): Upper Saddle River, N.J., Prentice Hall.
- Komar, P.D., and Inman, D., 1970, Longshore sand transport on beaches: *Journal of Geophysical Research—Oceans*, v. 70, no. 30, p. 5914–5927.
- Komen, G.J., Hasselmann, S., and Hasselmann, K., 1984, On the existence of a fully developed wind-sea spectrum: *Journal of Physical Oceanography*, v. 14, no. 8, p. 1271–1285.
- Kraus, N.C., and Galgano, F.A., 2001, Beach erosional hot spots—Types, causes, and solutions: U.S. Army Corps of Engineers, ERDC/CHL CHETN-II-44.
- Lavoie, D., Flocks, J., Kindinger, J., Sallenger, A., and Twichell, D., 2010, Effects of building a sand barrier berm to mitigate the effects of the Deepwater Horizon oil spill on Louisiana marshes: U.S. Geological Survey Open-File Report 2010–1108, 14 p.
- Long, J., Plant, N., Dalyander, P.S., and Thompson, D., 2014, A probabilistic method for constructing wave time-series at inshore locations using model scenarios: *Coastal Engineering*, v. 89, p. 53–62.
- Longuet-Higgins, M., 1952, On the statistical distribution of the height of sea waves: *Journal of Marine Research*, v. 11, p. 245–266.
- Longuet-Higgins, M., 1972, Recent progress in the study of longshore currents, *in* Meyer, R.E., ed., *Waves on beaches*: New York, Academic Press, p. 203–248.
- Love, M.R., Amante, C.J., Eakins, B.W., and Taylor, L.A., 2012, Digital elevation models of the Northern Gulf Coast—Procedures, data sources and analysis: Boulder, Colo., U.S. Department of Commerce, NOAA Technical Memorandum NESDIS NGDC-59, 43 p.

- Maa, J.P.Y., and Hobbs, C.H., III, 1998, Physical impact of waves on adjacent coasts resulting from dredging at Sandbridge Shoal, Virginia: *Journal of Coastal Research*, v. 14, no. 2, p. 525–536.
- Madsen, P.A., and Sørensen, O.R., 1993, Bound waves and triad interactions in shallow water: *Ocean Engineering*, v. 20, no. 4, p. 359–388.
- Martinez, L., O'Brien, S., Bethel, M., Penland, S., and Kulp, M., 2009, Louisiana barrier-island comprehensive monitoring program (BICM), Volume 2—Shoreline changes and barrier-island land loss 1880s to 2005: Prepared for the Louisiana Department of Natural Resources, Coastal Restoration Division by the University of New Orleans, Pontchartrain Institute for Environmental Sciences, New Orleans, La., 32 p.
- Michalsen, D., Haller, M., and Suh, K., 2008, Wave reflection from nearshore depressions: *Journal of Waterway, Port, Coastal, and Ocean Engineering*, v. 134, no. 1, p. 1–11.
- Miner, M., Kulp, M., Penland, S., Weathers, D., Motti, J.P., McCarty, P., and Reynolds, B.J., 2009, Louisiana Barrier Island Comprehensive Monitoring Program (BICM), Volume 3—Bathymetry and Historical Seafloor Change 1869–2007: Prepared for the Louisiana Department of Natural Resources, Coastal Restoration Division by the University of New Orleans, Pontchartrain Institute for Environmental Sciences, New Orleans, La., 16 p.
- Plant, N.G., Flocks, J., Stockdon, H.F., Long, J.W., Guy, K., Thompson, D.M., Cormier, J.M., Smith, C.G., Miselis, J.L., and Dalyander, P.S., 2014, Predictions of barrier island berm evolution in a time-varying storm climatology: *Journal of Geophysical Research Earth Surface*, v. 119, no. 2, p. 300–316.
- Plant, N.G., Holland, K.T., and Puleo, J.A., 2002, Analysis of the scale of errors in nearshore bathymetric data: *Marine Geology*, v. 191, no. 1, p. 71–86.
- Plant, N.G., Long, J.W., Dalyander, P.S., Thompson, D.M., and Raabe, E.A., 2013, Application of a hydrodynamic and sediment transport model for guidance of response efforts related to the Deepwater Horizon oil spill in the Northern Gulf of Mexico along the coast of Alabama and Florida: U.S. Geological Survey Open-File Report 2012–1234, 46 p., accessed February 13, 2015 at <http://pubs.usgs.gov/of/2012/1234/>.
- Reniers, A.J.H.M., Thornton, E.B., Stanton, T.P., and Roelvink, J.A., 2004, Vertical flow structure during Sandy Duck—Observations and modeling: *Coastal Engineering*, v. 51, p. 237–260.
- Ris, R.C., Holthuijsen, L.H., and Booij, N., 1999, A third-generation wave model for coastal regions—2. Verification: *Journal of Geophysical Research*, v. 104, no. C4, p. 7667–7681.
- Rogers, W.E., Hwang, P.A., and Wang, D.W., 2003, Investigation of wave growth and decay in the SWAN Model—Three regional-scale applications: *Journal of Physical Oceanography*, v. 33, p. 366–389.
- Rosati J., Walton T.L., and Bodge K., 2002, Longshore sediment transport—Coastal engineering manual, Part III, Coastal Sediment Processes Chapters 2–3: U.S. Army Corps of Engineers, Engineering Manual (EM) 1110-2-1100.
- The SWAN Team, 2014, SWAN—User Manual, SWAN Cycle III Version 41.01: Delft, The Netherlands, Delft University of Technology.

- Tolman, H.L., 2008, A mosaic approach to wind wave modeling: *Ocean Modeling*, v. 25, nos. 1–2, p. 35–47.
- Twichell, D., Pendleton, E., Baldwin, W., and Flocks, J., 2009, Geologic mapping of distribution and volume of potential resources, chap. E, *in* Lavoie, D., ed., Sand resources, regional geology, and coastal processes of the Chandeleur Islands coastal system—An evaluation of the Breton National Wildlife Refuge: U.S. Geological Survey Scientific Investigations Report 2009–5252, p. 75–98.
- Wang, Z., and Dean, R.G., 2001, Manatee County beach nourishment project performance and erosional hot spot analysis: University of Florida, UFL/COEL-2001/003.
- Zarillo, G., Zarillo, K., and Finnegan, C., 2009, Physical characterization of nearshore and offshore borrow sites on the Inner Continental Shelf of northeast and west Florida: *Journal of Coastal Research*, Special Issue 56, p. 1095–1099.

Appendix 1. Scenarios

This file contains information on 128 individual wave condition scenarios that were modeled in order to provide guidance on impacts of potential proposed sediment borrow pits on Breton Island wave climate

The columns in the table are:

Scenario: scenario name, assigned by USGS

Wave Height Bin (m): the range of wave heights this scenario represents

Wave Dir. Bin (meteorological convention, degs.): the wave directions this scenario represents (in degrees clockwise from north, direction waves are coming from)

% of Obs.: the percentage of observations between May, 1995, and December, 2013 that this scenario represents

Representative Time: specific time which that was modeled for the scenario

Scenario	Wave Height Bin Range (m)	Wave Direction Bin Range (degs. from N, waves coming from)	Percentage of Observations	Representative Time
H1_D1	0-0.5	0.00-22.50	0.73	10/21/2010 21:00
H1_D2	0-0.5	22.50-45.00	0.53	10/9/2005 21:00
H1_D3	0-0.5	45.00-67.50	0.86	10/1/2009 0:00
H1_D4	0-0.5	67.50-90.00	1.1	7/18/2008 6:00
H1_D5	0-0.5	90.00-112.50	1.45	8/26/2011 3:00
H1_D6	0-0.5	112.50-135.00	1.81	9/3/2010 21:00
H1_D7	0-0.5	135.00-157.50	3.73	3/16/2012 12:00
H1_D8	0-0.5	157.50-180.00	4.67	6/8/2010 18:00
H1_D9	0-0.5	180.00-202.50	2.23	6/13/2010 3:00
H1_D10	0-0.5	202.50-225.00	1.39	8/7/2008 0:00
H1_D11	0-0.5	225.00-247.50	1.02	7/24/2009 12:00
H1_D12	0-0.5	247.50-270.00	0.46	3/26/2012 12:00
H1_D13	0-0.5	270.00-292.50	0.48	8/15/2011 9:00
H1_D14	0-0.5	292.50-315.00	0.49	7/15/2010 0:00
H1_D15	0-0.5	315.00-337.50	0.47	7/31/2010 3:00
H1_D16	0-0.5	337.50-360.00	0.44	1/14/2012 18:00
H2_D1	0.5-1	0.00-22.50	1.06	9/30/2009 6:00
H2_D2	0.5-1	22.50-45.00	1.34	12/30/2008 6:00
H2_D3	0.5-1	45.00-67.50	2.41	12/8/2011 21:00
H2_D4	0.5-1	67.50-90.00	2.48	7/24/2007 9:00
H2_D5	0.5-1	90.00-112.50	3.4	1/20/2013 9:00
H2_D6	0.5-1	112.50-135.00	3.51	3/13/2007 3:00
H2_D7	0.5-1	135.00-157.50	6.3	7/20/2010 12:00
H2_D8	0.5-1	157.50-180.00	5.18	5/9/2009 3:00
H2_D9	0.5-1	180.00-202.50	2.5	7/10/2007 9:00
H2_D10	0.5-1	202.50-225.00	1.6	6/1/2012 6:00

Scenario	Wave Height Bin Range (m)	Wave Direction Bin Range (degs. from N, waves coming from)	Percentage of Observations	Representative Time
H2_D11	0.5-1	225.00-247.50	1.1	12/21/2008 12:00
H2_D12	0.5-1	247.50-270.00	0.5	8/2/2008 12:00
H2_D13	0.5-1	270.00-292.50	0.44	8/16/2010 0:00
H2_D14	0.5-1	292.50-315.00	0.42	10/31/2012 18:00
H2_D15	0.5-1	315.00-337.50	0.53	3/5/2012 0:00
H2_D16	0.5-1	337.50-360.00	0.88	11/11/2005 3:00
H3_D1	1-1.5	0.00-22.50	1.16	9/25/2006 15:00
H3_D2	1-1.5	22.50-45.00	1.28	1/19/2007 18:00
H3_D3	1-1.5	45.00-67.50	1.66	12/24/2010 6:00
H3_D4	1-1.5	67.50-90.00	1.41	8/11/2010 0:00
H3_D5	1-1.5	90.00-112.50	2.85	1/18/2007 12:00
H3_D6	1-1.5	112.50-135.00	2.6	10/26/2006 21:00
H3_D7	1-1.5	135.00-157.50	4.14	4/29/2009 9:00
H3_D8	1-1.5	157.50-180.00	2.78	6/29/2010 0:00
H3_D9	1-1.5	180.00-202.50	1.37	6/4/2010 3:00
H3_D10	1-1.5	202.50-225.00	0.68	1/9/2006 9:00
H3_D11	1-1.5	225.00-247.50	0.38	10/28/2010 0:00
H3_D12	1-1.5	247.50-270.00	0.17	1/19/2009 3:00
H3_D13	1-1.5	270.00-292.50	0.13	1/19/2009 6:00
H3_D14	1-1.5	292.50-315.00	0.24	3/1/2005 6:00
H3_D15	1-1.5	315.00-337.50	0.54	11/30/2005 6:00
H3_D16	1-1.5	337.50-360.00	1.03	2/8/2011 12:00
H4_D1	1.5-2	0.00-22.50	0.71	4/5/2011 18:00
H4_D2	1.5-2	22.50-45.00	0.72	1/16/2009 9:00
H4_D3	1.5-2	45.00-67.50	0.76	10/30/2011 6:00
H4_D4	1.5-2	67.50-90.00	0.71	10/12/2008 15:00
H4_D5	1.5-2	90.00-112.50	1.65	10/8/2007 15:00
H4_D6	1.5-2	112.50-135.00	1.5	3/24/2009 12:00
H4_D7	1.5-2	135.00-157.50	2.19	12/9/2008 18:00
H4_D8	1.5-2	157.50-180.00	1.15	2/12/2009 9:00
H4_D9	1.5-2	180.00-202.50	0.69	2/14/2012 21:00
H4_D10	1.5-2	202.50-225.00	0.2	12/24/2012 15:00
H4_D11	1.5-2	225.00-247.50	0.16	1/12/2012 18:00
H4_D12	1.5-2	247.50-270.00	0.04	11/29/2011 18:00
H4_D13	1.5-2	270.00-292.50	0.13	12/1/2008 18:00
H4_D14	1.5-2	292.50-315.00	0.19	2/5/2006 0:00
H4_D15	1.5-2	315.00-337.50	0.53	2/2/2011 12:00
H4_D16	1.5-2	337.50-360.00	0.8	12/4/2006 3:00
H5_D1	2.0-3.0	0.00-22.50	0.51	11/21/2008 15:00
H5_D2	2.0-3.0	22.50-45.00	0.37	12/4/2006 15:00
H5_D3	2.0-3.0	45.00-67.50	0.29	10/28/2007 12:00

Scenario	Wave Height Bin Range (m)	Wave Direction Bin Range (degs. from N, waves coming from)	Percentage of Observations	Representative Time
H5_D4	2.0-3.0	67.50-90.00	0.38	12/17/2005 18:00
H5_D5	2.0-3.0	90.00-112.50	1.15	10/4/2005 0:00
H5_D6	2.0-3.0	112.50-135.00	1.04	11/6/2006 9:00
H5_D7	2.0-3.0	135.00-157.50	1.23	3/6/2011 3:00
H5_D8	2.0-3.0	157.50-180.00	0.64	10/18/2006 6:00
H5_D9	2.0-3.0	180.00-202.50	0.47	2/14/2012 12:00
H5_D10	2.0-3.0	202.50-225.00	0.2	1/7/2009 9:00
H5_D11	2.0-3.0	225.00-247.50	0.15	1/11/2012 15:00
H5_D12	2.0-3.0	247.50-270.00	0.05	3/28/2005 6:00
H5_D13	2.0-3.0	270.00-292.50	0.12	12/1/2008 6:00
H5_D14	2.0-3.0	292.50-315.00	0.3	2/18/2007 6:00
H5_D15	2.0-3.0	315.00-337.50	0.6	12/21/2012 3:00
H5_D16	2.0-3.0	337.50-360.00	0.63	3/24/2006 9:00
H6_D1	3.0-4.0	0.00-22.50	0.06	11/17/2005 9:00
H6_D2	3.0-4.0	22.50-45.00	0.03	12/8/2006 9:00
H6_D3	3.0-4.0	45.00-67.50	0.02	1/19/2008 21:00
H6_D4	3.0-4.0	67.50-90.00	0.07	6/25/2012 6:00
H6_D5	3.0-4.0	90.00-112.50	0.23	12/8/2005 12:00
H6_D6	3.0-4.0	112.50-135.00	0.19	4/30/2006 3:00
H6_D7	3.0-4.0	135.00-157.50	0.18	4/30/2006 21:00
H6_D8	3.0-4.0	157.50-180.00	0.11	5/3/2010 6:00
H6_D9	3.0-4.0	180.00-202.50	0.14	3/10/2006 3:00
H6_D10	3.0-4.0	202.50-225.00	0.07	12/26/2012 6:00
H6_D11	3.0-4.0	225.00-247.50	0.05	12/26/2012 6:00
H6_D12	3.0-4.0	247.50-270.00	0.02	12/12/2008 0:00
H6_D13	3.0-4.0	270.00-292.50	0.02	12/12/2008 0:00
H6_D14	3.0-4.0	292.50-315.00	0.05	12/12/2008 0:00
H6_D15	3.0-4.0	315.00-337.50	0.06	12/26/2010 0:00
H6_D16	3.0-4.0	337.50-360.00	0.04	12/26/2010 0:00
H7_D1	4.0-5.0	0.00-22.50	0.01	10/24/2005 12:00
H7_D2	4.0-5.0	22.50-45.00	0.01	12/8/2006 9:00
H7_D3	4.0-5.0	45.00-67.50	0	
H7_D4	4.0-5.0	67.50-90.00	0.01	12/8/2005 15:00
H7_D5	4.0-5.0	90.00-112.50	0.05	12/8/2005 15:00
H7_D6	4.0-5.0	112.50-135.00	0.03	9/1/2008 21:00
H7_D7	4.0-5.0	135.00-157.50	0.04	9/22/2005 15:00
H7_D8	4.0-5.0	157.50-180.00	0.04	9/3/2011 9:00
H7_D9	4.0-5.0	180.00-202.50	0.03	9/5/2011 9:00
H7_D10	4.0-5.0	202.50-225.00	0.004	8/30/2005 3:00
H7_D11	4.0-5.0	225.00-247.50	0.01	8/30/2005 3:00
H7_D12	4.0-5.0	247.50-270.00	0.004	8/30/2005 3:00

Scenario	Wave Height Bin Range (m)	Wave Direction Bin Range (degs. from N, waves coming from)	Percentage of Observations	Representative Time
H7_D13	4.0-5.0	270.00-292.50	0	
H7_D14	4.0-5.0	292.50-315.00	0	
H7_D15	4.0-5.0	315.00-337.50	0	
H7_D16	4.0-5.0	337.50-360.00	0	
H8_D1	5.0-6.0	0.00-22.50	0.001	8/29/2005 12:00
H8_D2	5.0-6.0	22.50-45.00	0	
H8_D3	5.0-6.0	45.00-67.50	0	
H8_D4	5.0-6.0	67.50-90.00	0	
H8_D5	5.0-6.0	90.00-112.50	0.04	9/1/2008 12:00
H8_D6	5.0-6.0	112.50-135.00	0.04	9/1/2008 15:00
H8_D7	5.0-6.0	135.00-157.50	0.02	8/28/2005 21:00
H8_D8	5.0-6.0	157.50-180.00	0.02	9/12/2008 12:00
H8_D9	5.0-6.0	180.00-202.50	0.003	8/29/2005 15:00
H8_D10	5.0-6.0	202.50-225.00	0.01	8/29/2005 18:00
H8_D11	5.0-6.0	225.00-247.50	0.01	8/29/2005 18:00
H8_D12	5.0-6.0	247.50-270.00	0.003	8/29/2005 12:00
H8_D13	5.0-6.0	270.00-292.50	0	
H8_D14	5.0-6.0	292.50-315.00	0	
H8_D15	5.0-6.0	315.00-337.50	0	
H8_D16	5.0-6.0	337.50-360.00	0	

Appendix 2. Example Model Input Files

Example SWAN input files for each of the four grids (G1–G4) are provided in this appendix. The example provided is for scenarios H1_D1 (wave height bin 1, direction bin 1). Other scenarios would vary in the forcing input wind file used. For grid 4, the example given is for the baseline case of no borrow pit; cases with borrow pits use a different bathymetry file incorporating the proposed pit design.

Grid G1:

```
PROJECT 'Breton' \ \
'G1'
'H1_D1'
'21-Oct-2010 21:00:00'

MODE STATIONARY TWODIMENSIONAL
SET DEPMIN 0.20 INRHOG 1 NAUTICAL PWTAIL 5
COORDINATES CARTESIAN

&& KEYWORDS TO CREATE AND READ COMPUTATIONAL GRID &&
CGRID CURVILINEAR 324 103 EXC 9.999000e+003 &
    CIRCLE 60 0.04 1.0
READGRID COORDINATES 1 'C:\Users\rmickey\Documents\SWAN_ngomex\breton\grids\
NGMexG1v2.grd' 4 0 0 FREE
```

```

&& KEYWORDS TO CREATE AND READ BATHYMETRY GRID &&
INPGRID BOTTOM CURVILINEAR 0 0 324 103 EXC 9.999000e+003
READINP BOTTOM 1 'C:\Users\rmickey\Documents\SWAN_ngomex\breton\grids\NG-
MexGlv2.bot' 4 0 FREE

&& KEYWORD TO CREATE CURRENT GRID &&
$INPGRID CURRENT CURVILINEAR 0 0 500 135 EXC 9.999000e+003      &
$      NONSTAT 20100801.000000 1 DAY 20100901.000000

&& KEYWORD TO CREATE WATER LEVEL GRID &&
$INPGRID WLEV CURVILINEAR 0 0 500 135 EXC 9.999000e+003      &
$      NONSTAT 20100801.000000 1 DAY 20100901.000000

&& KEYWORD TO CREATE BOTTOM FRICTION GRID &&
$INPGRID FRIC CURVILINEAR 0 0 500 135 EXC 9.999000e+003      &
$      NONSTAT 20100801.000000 1 DAY 20100901.000000

&& Wind forcing &&
INPGRID WIND REGULAR 155000.0 3200000.0 0 92 32 6350.0 7400.0 EXC
9.999000e+003
READINP WIND 1 'C:\Users\rmickey\Documents\SWAN_ngomex\breton\forcings\swan_
wind\H1_D1_wind.dat' 4 0 FREE

&& BOUNDARY FORCING &&
BOUND SHAPE JONSWAP 3.3 PEAK DSPR DEGREES

BOUNDSPEC SEGMENT IJ 0 0 2 0 CONSTANT PAR 0.1 5.1 127.7 20.0
BOUNDSPEC SEGMENT IJ 2 0 5 0 CONSTANT PAR 0.1 5.1 130.2 20.0
BOUNDSPEC SEGMENT IJ 5 0 9 0 CONSTANT PAR 0.1 5.2 132.4 20.0
BOUNDSPEC SEGMENT IJ 9 0 13 0 CONSTANT PAR 0.0 5.2 139.7 20.0
BOUNDSPEC SEGMENT IJ 13 0 17 0 CONSTANT PAR 0.0 5.2 139.7 20.0
BOUNDSPEC SEGMENT IJ 17 0 21 0 CONSTANT PAR 0.0 5.2 157.8 20.0
BOUNDSPEC SEGMENT IJ 21 0 25 0 CONSTANT PAR 0.0 5.2 193.2 20.0
BOUNDSPEC SEGMENT IJ 25 0 29 0 CONSTANT PAR 0.0 5.1 219.6 20.0
BOUNDSPEC SEGMENT IJ 29 0 33 0 CONSTANT PAR 0.0 5.1 228.8 20.0
BOUNDSPEC SEGMENT IJ 33 0 37 0 CONSTANT PAR 0.0 4.8 232.9 20.0
BOUNDSPEC SEGMENT IJ 37 0 41 0 CONSTANT PAR 0.1 4.3 232.9 20.0
BOUNDSPEC SEGMENT IJ 41 0 45 0 CONSTANT PAR 0.1 3.4 260.0 20.0
BOUNDSPEC SEGMENT IJ 45 0 49 0 CONSTANT PAR 0.1 3.9 170.3 20.0
BOUNDSPEC SEGMENT IJ 49 0 53 0 CONSTANT PAR 0.1 4.2 170.3 20.0
BOUNDSPEC SEGMENT IJ 53 0 57 0 CONSTANT PAR 0.1 4.1 52.9 20.0
BOUNDSPEC SEGMENT IJ 57 0 61 0 CONSTANT PAR 0.3 2.7 45.1 20.0
BOUNDSPEC SEGMENT IJ 61 0 65 0 CONSTANT PAR 0.2 2.9 39.2 20.0
BOUNDSPEC SEGMENT IJ 65 0 69 0 CONSTANT PAR 0.2 3.2 34.2 20.0
BOUNDSPEC SEGMENT IJ 69 0 73 0 CONSTANT PAR 0.3 3.2 34.2 20.0
BOUNDSPEC SEGMENT IJ 73 0 77 0 CONSTANT PAR 0.3 3.2 31.4 20.0
BOUNDSPEC SEGMENT IJ 77 0 81 0 CONSTANT PAR 0.3 3.2 29.3 20.0
BOUNDSPEC SEGMENT IJ 81 0 85 0 CONSTANT PAR 0.3 3.2 27.4 20.0
BOUNDSPEC SEGMENT IJ 85 0 89 0 CONSTANT PAR 0.3 3.2 25.6 20.0
BOUNDSPEC SEGMENT IJ 89 0 93 0 CONSTANT PAR 0.3 3.2 23.7 20.0

```

BOUNDSPEC	SEGMENT	IJ	93	0	97	0	CONSTANT	PAR	0.3	3.2	21.5	20.0
BOUNDSPEC	SEGMENT	IJ	97	0	101	0	CONSTANT	PAR	0.3	3.1	19.1	20.0
BOUNDSPEC	SEGMENT	IJ	101	0	105	0	CONSTANT	PAR	0.3	3.1	16.5	20.0
BOUNDSPEC	SEGMENT	IJ	105	0	109	0	CONSTANT	PAR	0.3	3.1	13.7	20.0
BOUNDSPEC	SEGMENT	IJ	109	0	113	0	CONSTANT	PAR	0.3	3.1	10.8	20.0
BOUNDSPEC	SEGMENT	IJ	113	0	117	0	CONSTANT	PAR	0.3	3.1	8.2	20.0
BOUNDSPEC	SEGMENT	IJ	117	0	121	0	CONSTANT	PAR	0.3	3.2	8.2	20.0
BOUNDSPEC	SEGMENT	IJ	121	0	125	0	CONSTANT	PAR	0.3	3.2	6.4	20.0
BOUNDSPEC	SEGMENT	IJ	125	0	129	0	CONSTANT	PAR	0.3	3.3	5.7	20.0
BOUNDSPEC	SEGMENT	IJ	129	0	133	0	CONSTANT	PAR	0.3	3.3	6.1	20.0
BOUNDSPEC	SEGMENT	IJ	133	0	137	0	CONSTANT	PAR	0.4	3.4	15.1	20.0
BOUNDSPEC	SEGMENT	IJ	137	0	141	0	CONSTANT	PAR	0.4	3.4	14.3	20.0
BOUNDSPEC	SEGMENT	IJ	141	0	145	0	CONSTANT	PAR	0.4	3.4	13.6	20.0
BOUNDSPEC	SEGMENT	IJ	145	0	149	0	CONSTANT	PAR	0.4	3.4	13.1	20.0
BOUNDSPEC	SEGMENT	IJ	149	0	153	0	CONSTANT	PAR	0.4	3.4	13.3	20.0
BOUNDSPEC	SEGMENT	IJ	153	0	157	0	CONSTANT	PAR	0.4	3.4	14.6	20.0
BOUNDSPEC	SEGMENT	IJ	157	0	161	0	CONSTANT	PAR	0.4	3.4	16.4	20.0
BOUNDSPEC	SEGMENT	IJ	161	0	165	0	CONSTANT	PAR	0.4	3.3	13.1	20.0
BOUNDSPEC	SEGMENT	IJ	165	0	169	0	CONSTANT	PAR	0.4	3.3	12.0	20.0
BOUNDSPEC	SEGMENT	IJ	169	0	173	0	CONSTANT	PAR	0.4	3.3	10.7	20.0
BOUNDSPEC	SEGMENT	IJ	173	0	177	0	CONSTANT	PAR	0.4	3.3	10.7	20.0
BOUNDSPEC	SEGMENT	IJ	177	0	181	0	CONSTANT	PAR	0.4	3.3	9.6	20.0
BOUNDSPEC	SEGMENT	IJ	181	0	185	0	CONSTANT	PAR	0.4	3.3	8.4	20.0
BOUNDSPEC	SEGMENT	IJ	185	0	189	0	CONSTANT	PAR	0.4	3.3	7.4	20.0
BOUNDSPEC	SEGMENT	IJ	189	0	193	0	CONSTANT	PAR	0.4	3.3	6.2	20.0
BOUNDSPEC	SEGMENT	IJ	193	0	197	0	CONSTANT	PAR	0.4	3.3	4.9	20.0
BOUNDSPEC	SEGMENT	IJ	197	0	201	0	CONSTANT	PAR	0.4	3.3	3.4	20.0
BOUNDSPEC	SEGMENT	IJ	201	0	205	0	CONSTANT	PAR	0.4	3.3	1.6	20.0
BOUNDSPEC	SEGMENT	IJ	205	0	209	0	CONSTANT	PAR	0.4	3.3	359.6	20.0
BOUNDSPEC	SEGMENT	IJ	209	0	213	0	CONSTANT	PAR	0.4	3.3	357.5	20.0
BOUNDSPEC	SEGMENT	IJ	213	0	217	0	CONSTANT	PAR	0.4	3.3	355.5	20.0
BOUNDSPEC	SEGMENT	IJ	217	0	221	0	CONSTANT	PAR	0.4	3.3	353.6	20.0
BOUNDSPEC	SEGMENT	IJ	221	0	225	0	CONSTANT	PAR	0.4	3.3	351.7	20.0
BOUNDSPEC	SEGMENT	IJ	225	0	229	0	CONSTANT	PAR	0.4	3.3	351.7	20.0
BOUNDSPEC	SEGMENT	IJ	229	0	233	0	CONSTANT	PAR	0.4	3.3	349.6	20.0
BOUNDSPEC	SEGMENT	IJ	233	0	237	0	CONSTANT	PAR	0.4	3.3	347.3	20.0
BOUNDSPEC	SEGMENT	IJ	237	0	241	0	CONSTANT	PAR	0.4	3.3	344.7	20.0
BOUNDSPEC	SEGMENT	IJ	241	0	245	0	CONSTANT	PAR	0.3	3.3	342.0	20.0
BOUNDSPEC	SEGMENT	IJ	245	0	249	0	CONSTANT	PAR	0.3	3.3	339.1	20.0
BOUNDSPEC	SEGMENT	IJ	249	0	253	0	CONSTANT	PAR	0.3	3.3	336.3	20.0
BOUNDSPEC	SEGMENT	IJ	253	0	257	0	CONSTANT	PAR	0.3	3.3	333.6	20.0
BOUNDSPEC	SEGMENT	IJ	257	0	261	0	CONSTANT	PAR	0.3	3.3	331.1	20.0
BOUNDSPEC	SEGMENT	IJ	261	0	265	0	CONSTANT	PAR	0.3	3.4	319.8	20.0
BOUNDSPEC	SEGMENT	IJ	265	0	269	0	CONSTANT	PAR	0.3	3.4	317.3	20.0
BOUNDSPEC	SEGMENT	IJ	269	0	273	0	CONSTANT	PAR	0.3	3.5	315.0	20.0
BOUNDSPEC	SEGMENT	IJ	273	0	277	0	CONSTANT	PAR	0.3	3.5	312.9	20.0
BOUNDSPEC	SEGMENT	IJ	277	0	281	0	CONSTANT	PAR	0.3	3.6	310.7	20.0
BOUNDSPEC	SEGMENT	IJ	281	0	285	0	CONSTANT	PAR	0.3	3.6	310.7	20.0
BOUNDSPEC	SEGMENT	IJ	285	0	289	0	CONSTANT	PAR	0.3	3.7	308.6	20.0

```

BOUNDSPEC SEGMENT IJ 289 0 293 0 CONSTANT PAR 0.3 3.7 296.7 20.0
BOUNDSPEC SEGMENT IJ 293 0 297 0 CONSTANT PAR 0.3 3.7 294.8 20.0
BOUNDSPEC SEGMENT IJ 297 0 301 0 CONSTANT PAR 0.3 3.8 293.2 20.0
BOUNDSPEC SEGMENT IJ 301 0 305 0 CONSTANT PAR 0.3 3.8 291.9 20.0
BOUNDSPEC SEGMENT IJ 305 0 309 0 CONSTANT PAR 0.3 3.9 290.8 20.0
BOUNDSPEC SEGMENT IJ 309 0 313 0 CONSTANT PAR 0.3 3.9 289.9 20.0
BOUNDSPEC SEGMENT IJ 313 0 317 0 CONSTANT PAR 0.3 3.9 289.0 20.0
BOUNDSPEC SEGMENT IJ 317 0 322 0 CONSTANT PAR 0.3 4.0 288.2 20.0
BOUNDSPEC SEGMENT IJ 322 0 324 0 CONSTANT PAR 0.3 4.1 278.9 20.0
BOUNDSPEC SEGMENT IJ 324 0 324 2 CONSTANT PAR 0.3 4.1 278.9 20.0
BOUNDSPEC SEGMENT IJ 324 2 324 5 CONSTANT PAR 0.3 4.1 278.9 20.0
BOUNDSPEC SEGMENT IJ 324 5 324 9 CONSTANT PAR 0.3 4.0 276.9 20.0
BOUNDSPEC SEGMENT IJ 324 9 324 13 CONSTANT PAR 0.3 4.0 282.9 20.0
BOUNDSPEC SEGMENT IJ 324 13 324 17 CONSTANT PAR 0.2 4.0 280.3 20.0
BOUNDSPEC SEGMENT IJ 324 17 324 21 CONSTANT PAR 0.2 4.0 277.0 20.0
BOUNDSPEC SEGMENT IJ 324 21 324 25 CONSTANT PAR 0.2 4.1 277.0 20.0
BOUNDSPEC SEGMENT IJ 324 25 324 29 CONSTANT PAR 0.1 4.2 265.0 20.0
BOUNDSPEC SEGMENT IJ 324 29 324 33 CONSTANT PAR 0.0 4.4 255.8 20.0
BOUNDSPEC SEGMENT IJ 324 33 324 37 CONSTANT PAR 0.0 4.3 255.8 20.0
BOUNDSPEC SEGMENT IJ 324 37 324 41 CONSTANT PAR 0.0 4.3 255.8 20.0
BOUNDSPEC SEGMENT IJ 324 41 324 45 CONSTANT PAR 0.0 4.3 255.8 20.0
BOUNDSPEC SEGMENT IJ 324 45 324 49 CONSTANT PAR 0.0 3.5 255.8 20.0
BOUNDSPEC SEGMENT IJ 324 49 324 53 CONSTANT PAR 0.0 3.2 255.8 20.0
BOUNDSPEC SEGMENT IJ 324 53 324 57 CONSTANT PAR 0.0 3.1 231.0 20.0
BOUNDSPEC SEGMENT IJ 324 57 324 59 CONSTANT PAR 0.0 4.5 231.0 20.0

```

```

& Restart name *****
&INIT HOTSTART 'swan_restart.dat'

```

```

& PHYSICS *****
GEN3 KOMEN
PROP BSBT
WCAP KOM 2.36E-5 3.02E-3 2.0 1.0 1.0
FRICTION JONSWAP 0.067

```

```

POINTS 'NDBC' FILE &
'C:\Users\rmickey\Documents\SWAN_ngomex\breton\out_locs\buoys.loc'

```

```

NGRID 'NGMEXG2' 208000. 3246100. 0. 252000. 138900. 840 463

```

```

SPEC 'NDBC' SPEC2D ABSOLUTE 'ndbc_buoy.spc'
TABLE 'NDBC' HEAD 'ndbc_buoy.tab' &
TIME XP YP DEPTH HSIGN RTP PDIR TM02 DIR WIND

```

```

NESTOUT 'NGMEXG2' &
'C:\Users\rmickey\Documents\SWAN_ngomex\breton\forcings\nst_G2\G2_H1_
D1.nst'

```

```

BLOCK 'COMPGRID' NOHEADER 'hsig.mat' LAY 4 HSIGN 1.

```

```

BLOCK 'COMPGRID' NOHEADER 'rtp.mat' LAY 4 RTP 1.
BLOCK 'COMPGRID' NOHEADER 'tm02.mat' LAY 4 TM02 1.
BLOCK 'COMPGRID' NOHEADER 'pmdir.mat' LAY 4 PDIR 1.
BLOCK 'COMPGRID' NOHEADER 'mwdir.mat' LAY 4 DIR 1.
BLOCK 'COMPGRID' NOHEADER 'xp.mat' LAY 4 XP 1.
BLOCK 'COMPGRID' NOHEADER 'yp.mat' LAY 4 YP 1.

```

COMPUTE STATIONARY

\$HOTFILE '.swanP1208_restart.dat01'

STOP

Grid G2:

```

PROJECT 'Breton' ' '
'G2'
'H1_D1'
'21-Oct-2010 21:00:00'

```

```

MODE STATIONARY TWODIMENSIONAL
SET DEPMIN 0.20 INRHOG 1 NAUTICAL PWTAIL 5
COORDINATES CARTESIAN

```

```

&& KEYWORDS TO CREATE AND READ COMPUTATIONAL GRID &&
CGRID CURVILINEAR 840 463 EXC 9.999000e+003 &
  CIRCLE 60 0.04 1.0
READGRID COORDINATES 1 'C:\Users\rmickey\Documents\SWAN_ngomex\breton\grids\
NGMexG2.grd' 4 0 0 FREE

```

```

&& KEYWORDS TO CREATE AND READ BATHYMETRY GRID &&
INPGRID BOTTOM CURVILINEAR 0 0 840 463 EXC 9.999000e+003
READINP BOTTOM 1 'C:\Users\rmickey\Documents\SWAN_ngomex\breton\grids\NG-
MexG2.bot' 4 0 FREE

```

```

&& KEYWORD TO CREATE CURRENT GRID &&
$INPGRID CURRENT CURVILINEAR 0 0 500 135 EXC 9.999000e+003 &
$  NONSTAT 20100801.000000 1 DAY 20100901.000000

```

```

&& KEYWORD TO CREATE WATER LEVEL GRID &&
$INPGRID WLEV CURVILINEAR 0 0 500 135 EXC 9.999000e+003 &
$  NONSTAT 20100801.000000 1 DAY 20100901.000000

```

```

&& KEYWORD TO CREATE BOTTOM FRICTION GRID &&
$INPGRID FRIC CURVILINEAR 0 0 500 135 EXC 9.999000e+003 &
$  NONSTAT 20100801.000000 1 DAY 20100901.000000

```

```

&& Wind forcing &&
INPGRID WIND REGULAR 155000.0 3200000.0 0 92 32 6350.0 7400.0 EXC
9.999000e+003

```

```

READINP WIND 1 'C:\Users\rmickey\Documents\SWAN_ngomex\breton\forcings\swan_
wind\H1_D1_wind.dat' 4 0 FREE

&& BOUNDARY FORCING &&
BOUN NEST &
'C:\Users\rmickey\Documents\SWAN_ngomex\breton\forcings\nst_G2\G2_H1_D1.nst'
CLOSED

& Restart name *****
&INIT HOTSTART 'swan_restart.dat'

& PHYSICS *****
GEN3 KOMEN
PROP BSBT
WCAP KOM 2.36E-5 3.02E-3 2.0 1.0 1.0
FRICTION JONSWAP 0.067

POINTS 'NDBC' FILE &
'C:\Users\rmickey\Documents\SWAN_ngomex\breton\out_locs\buoys.loc'

NGRID 'NGMEXG3' 277400. 3251750. 0. 32700. 19440. 545 324

SPEC 'NDBC' SPEC2D ABSOLUTE 'ndbc_buoy.spc'
TABLE 'NDBC' HEAD 'ndbc_buoy.tab' &
    TIME XP YP DEPTH HSIGN RTP PDIR TM02 DIR WIND

NESTOUT 'NGMEXG3' &
'C:\Users\rmickey\Documents\SWAN_ngomex\breton\forcings\nst_G3\G3_H1_
D1.nst'

BLOCK 'COMPGRID' NOHEADER 'hsig.mat' LAY 4 HSIGN 1.
BLOCK 'COMPGRID' NOHEADER 'rtp.mat' LAY 4 RTP 1.
BLOCK 'COMPGRID' NOHEADER 'tm02.mat' LAY 4 TM02 1.
BLOCK 'COMPGRID' NOHEADER 'pmdir.mat' LAY 4 PDIR 1.
BLOCK 'COMPGRID' NOHEADER 'mwdir.mat' LAY 4 DIR 1.
BLOCK 'COMPGRID' NOHEADER 'xp.mat' LAY 4 XP 1.
BLOCK 'COMPGRID' NOHEADER 'yp.mat' LAY 4 YP 1.

COMPUTE STATIONARY

$HOTFILE '.swanP1208_restart.dat01'

STOP

```

Grid G3:

```
PROJECT 'Breton' ' '
'G3'
'H1_D1'
'21-Oct-2010 21:00:00'

MODE STATIONARY TWODIMENSIONAL
SET DEPMIN 0.05 INRHOG 1 NAUTICAL PWTAIL 5
COORDINATES CARTESIAN

&& KEYWORDS TO CREATE AND READ COMPUTATIONAL GRID &&
CGRID CURVILINEAR 545 324 EXC 9.999000e+003 &
    CIRCLE 60 0.04 1.0
READGRID COORDINATES 1 'C:\Users\rmickey\Documents\SWAN_ngomex\breton\grids\
NGMexG3.grd' 4 0 0 FREE

&& KEYWORDS TO CREATE AND READ BATHYMETRY GRID &&
INPGRID BOTTOM CURVILINEAR 0 0 545 324 EXC 9.999000e+003
READINP BOTTOM 1 'C:\Users\rmickey\Documents\SWAN_ngomex\breton\grids\NG-
MexG3.bot' 4 0 FREE

&& KEYWORD TO CREATE CURRENT GRID &&
$INPGRID CURRENT CURVILINEAR 0 0 500 135 EXC 9.999000e+003      &
$    NONSTAT 20100801.000000 1 DAY 20100901.000000

&& KEYWORD TO CREATE WATER LEVEL GRID &&
$INPGRID WLEV CURVILINEAR 0 0 500 135 EXC 9.999000e+003      &
$    NONSTAT 20100801.000000 1 DAY 20100901.000000

&& KEYWORD TO CREATE BOTTOM FRICTION GRID &&
$INPGRID FRIC CURVILINEAR 0 0 500 135 EXC 9.999000e+003      &
$    NONSTAT 20100801.000000 1 DAY 20100901.000000

&& Wind forcing &&
INPGRID WIND REGULAR 155000.0 3200000.0 0 92 32 6350.0 7400.0 EXC
9.999000e+003
READINP WIND 1 'C:\Users\rmickey\Documents\SWAN_ngomex\breton\forcings\swan_
wind\H1_D1_wind.dat' 4 0 FREE

&& BOUNDARY FORCING &&
BOUN NEST &
'C:\Users\rmickey\Documents\SWAN_ngomex\breton\forcings\nst_G3\G3_H1_D1.nst'
CLOSED

& Restart name *****
&INIT HOTSTART 'swan_restart.dat'

& PHYSICS *****
GEN3 KOMEN
```

```

PROP BSBT
WCAP KOM 2.36E-5 3.02E-3 2.0 1.0 1.0
FRICTION JONSWAP 0.067

TRIAD
POINTS 'NDBC' FILE &
'C:\Users\rmickey\Documents\SWAN_ngomex\breton\out_locs\buoys.loc'

NGRID 'NGMEXG4' 283660. 3256780. 0. 18220. 10820. 1024 541

SPEC 'NDBC' SPEC2D ABSOLUTE 'ndbc_buoy.spc'
TABLE 'NDBC' HEAD 'ndbc_buoy.tab' &
    TIME XP YP DEPTH HSIGN RTP PDIR TM02 DIR WIND

NESTOUT 'NGMEXG4' &
'C:\Users\rmickey\Documents\SWAN_ngomex\breton\forcings\nst_G4\G4_H1_
D1.nst'

BLOCK 'COMPGRID' NOHEADER 'hsig.mat' LAY 4 HSIGN 1.
BLOCK 'COMPGRID' NOHEADER 'rtp.mat' LAY 4 RTP 1.
BLOCK 'COMPGRID' NOHEADER 'tm02.mat' LAY 4 TM02 1.
BLOCK 'COMPGRID' NOHEADER 'pmdir.mat' LAY 4 PDIR 1.
BLOCK 'COMPGRID' NOHEADER 'mwdir.mat' LAY 4 DIR 1.
BLOCK 'COMPGRID' NOHEADER 'xp.mat' LAY 4 XP 1.
BLOCK 'COMPGRID' NOHEADER 'yp.mat' LAY 4 YP 1.

COMPUTE STATIONARY

$HOTFILE '.swanP1208_restart.dat01'

STOP

Grid G4:
PROJECT 'Breton' ' '
'G4'
'H1_D1'
'21-Oct-2010 21:00:00'

MODE STATIONARY TWODIMENSIONAL
SET DEPMIN 0.05 INRHOG 1 NAUTICAL PWTAIL 5
COORDINATES CARTESIAN

&& KEYWORDS TO CREATE AND READ COMPUTATIONAL GRID &&
CGRID CURVILINEAR 1024 541 EXC 9.999000e+003 &
    CIRCLE 60 0.04 1.0
READGRID COORDINATES 1 'C:\Users\rmickey\Documents\SWAN_ngomex\breton\grids\
NGMexG4.grd' 4 0 0 FREE

&& KEYWORDS TO CREATE AND READ BATHYMETRY GRID &&

```

```

INPGRID BOTTOM CURVILINEAR 0 0 1024 541 EXC 9.999000e+003
READINP BOTTOM 1 'C:\Users\rmickey\Documents\SWAN_ngomex\breton\grids\NG-
MexG4.bot' 4 0 FREE

&& KEYWORD TO CREATE CURRENT GRID &&
$INPGRID CURRENT CURVILINEAR 0 0 500 135 EXC 9.999000e+003      &
$  NONSTAT 20100801.000000 1 DAY 20100901.000000

&& KEYWORD TO CREATE WATER LEVEL GRID &&
$INPGRID WLEV CURVILINEAR 0 0 500 135 EXC 9.999000e+003      &
$  NONSTAT 20100801.000000 1 DAY 20100901.000000

&& KEYWORD TO CREATE BOTTOM FRICTION GRID &&
$INPGRID FRIC CURVILINEAR 0 0 500 135 EXC 9.999000e+003      &
$  NONSTAT 20100801.000000 1 DAY 20100901.000000

&& Wind forcing &&
INPGRID WIND REGULAR 155000.0 3200000.0 0 92 32 6350.0 7400.0 EXC
9.999000e+003
READINP WIND 1 'C:\Users\rmickey\Documents\SWAN_ngomex\breton\forcings\swan_
wind\H1_D1_wind.dat' 4 0 FREE

&& BOUNDARY FORCING &&
BOUN NEST &
'C:\Users\rmickey\Documents\SWAN_ngomex\breton\forcings\nst_G4\G4_H1_D1.nst'
CLOSED

& Restart name *****
&INIT HOTSTART 'swan_restart.dat'

& PHYSICS *****
GEN3 KOMEN
PROP BSBT
WCAP KOM 2.36E-5 3.02E-3 2.0 1.0 1.0
FRICTION JONSWAP 0.067

TRIAD
POINTS 'NDBC' FILE &
'C:\Users\rmickey\Documents\SWAN_ngomex\breton\out_locs\buoys.loc'

SPEC 'NDBC' SPEC2D ABSOLUTE 'ndbc_buoy.spc'
TABLE 'NDBC' HEAD 'ndbc_buoy.tab' &
  TIME XP YP DEPTH HSIGN RTP PDIR TM02 DIR WIND

BLOCK 'COMPGRID' NOHEADER 'hsig.mat' LAY 4 HSIGN 1.
BLOCK 'COMPGRID' NOHEADER 'rtp.mat' LAY 4 RTP 1.
BLOCK 'COMPGRID' NOHEADER 'tm02.mat' LAY 4 TM02 1.
BLOCK 'COMPGRID' NOHEADER 'pmdir.mat' LAY 4 PDIR 1.

```

```
BLOCK 'COMPGRID' NOHEADER 'mwdir.mat' LAY 4 DIR 1.  
BLOCK 'COMPGRID' NOHEADER 'xp.mat' LAY 4 XP 1.  
BLOCK 'COMPGRID' NOHEADER 'yp.mat' LAY 4 YP 1.
```

```
COMPUTE STATIONARY
```

```
$HOTFILE '.swanP1208_restart.dat01'
```

```
STOP
```

Appendix 3. File Naming Conventions

Model results from all four grids are available in geographic information systems (GIS) polygon shapefile format, with all files for a given scenario having a prefix of Gg_Hh_Dd, where g denotes the grid number (1, 2, 3, or 4), and h and d denote the scenario wave height (H) and direction (D) bin number, respectively. So, for example, a prefix of “G1_H1_D1” corresponds to output from grid G1 for a wave height in the lowest bin (0.0 to 0.5 meter) and wave direction in the first bin (0 to 22.5 degrees). A table of scenario characteristics is provided in appendix 1 and is also included in a text file (.txt) zipped with each GIS shapefile. In the case of grid G4, for cases where a borrow pit is included, there is an additional prefix “Pp” where p denotes which proposed borrow pit was considered (1 or 2; fig. 3). The final portion of the filename denotes the output type. For example, G1_H1_D1_wave_height.xxx would contain significant wave height for scenario H1_D1 for grid G1, with various file extensions (.xxx) associated with the GIS shapefile.

